AEDC-TR-73-168

EXPERIMENTAL STUDIES OF A LUDWIEG TUBE HIGH REYNOLDS NUMBER TRANSONIC TUNNEL

R. F. Starr and C. J. Schueler

ARO, Inc.

December 1973

VON KÁRMÁN GAS DYNAMICS FACILITY

ARNOLD ENGINEERING DEVELOPMENT CENTER

AIR FORCE SYSTEMS COMMAND

ARNOLD AIR FORCE STATION, TENNESSEE

NOTICES

When U. S. Government drawings specifications, or other data are used for any purpose other than a definitely related Government procurement operation, the Government thereby incurs no responsibility nor any obligation whatsoever, and the fact that the Government may have formulated, furnished, or in any way supplied the said drawings, specifications, or other data, is not to be regarded by implication or otherwise, or in any manner licensing the holder or any other person or corporation, or conveying any rights or permission to manufacture, use, or sell any patented invention that may in any way be related thereto.

Qualified users may obtain copies of this report from the Defense Documentation Center.

References to named commercial products in this report are not to be considered in any sense as an endorsement of the product by the United States Air Force or the Government.

EXPERIMENTAL STUDIES OF A LUDWIEG TUBE HIGH REYNOLDS NUMBER TRANSONIC TUNNEL

R. F. Starr and C. J. Schueler
ARO, Inc.

FOREWORD

The study reported herein was conducted by the Arnold Engineering Development Center (AEDC), Air Force Systems Command (AFSC), under Program Element 65802F.

This work was done by ARO, Inc. (a subsidiary of Sverdrup & Parcel and Associates, Inc.), contract operator of AEDC, Arnold Air Force Station, Tennessee. The research covered the period from July 1972 to February 1973, and the manuscript was submitted for publication on July 2, 1973. The ARO Project No. was VD209.

The authors wish to acknowledge the assistance of James C. Sivells, ARO, Inc., who modified Becker's theory to account for the high Reynolds number skin-friction coefficient, and Dr. Arloe Mayne, Jr., ARO, Inc., who provided the theoretical calculation of the turbulent boundary-layer growth on a flat plate with a starting profile similar to that at the charge tube exit. The series of experiments conducted in the NASA MSFC 14-in. transonic tunnel (Ref. 25) were carried out with the cooperation of Mr. A. R. Felix, Chief, Experimental Aerophysics Branch, NASA - Marshall Space Flight Center, Huntsville, Alabama.

This technical report has been reviewed and is approved.

FORREST B. SMITH
Facility Development Division
Directorate of Civil Engineering

R. R. GARREN
Colonel, USAF
Director of Civil Engineering

ABSTRACT

A significant justification for a much higher Reynolds number ground test capability in the transonic regime has developed in the past few years. An extensive experimental investigation of a high Reynolds number transonic wind tunnel employing a Ludwieg tube air storage system has been undertaken at the Arnold Engineering Development Center to assess the utility of such a device. The transonic starting process and starting time of this impulse facility have been carefully evaluated, and the spatial and timewise quality of the test section flow has been analyzed. Results from studies of the aerodynamic flow response time at transonic speeds and measurement of the pressure distribution and forces on selected models are presented. Also included are the results from associated studies of the influence of plenum volume on test section flow quality and the acoustic environment of the tunnel exhaust.

CONTENTS

ILLUSTRATIONS

NOMENCLATURE

A	Cross-sectional area
A^*	Cross-sectional area at sonic point
A_M	Main starting device effective open area
A_{PE}	Plenum exhaust effective open area
A_W	Porous wall effective open area
a	Speed of sound
a_{4a}	Speed of sound behind unsteady wave in charge tube
b	Vehicle wing span
C_D	Total drag coefficient, $\text{drag}/q_\infty S_b$
C_{D_B}	Base drag coefficient, $(p_\infty - p_B)/q_\infty$
C_{D_F}	Forebody drag coefficient, $C_D - C_{D_B}$
C_p^*	Sonic pressure coefficient
C_{p_u}	Pressure coefficient on upper surface, $(p_L - p_\infty)/q_\infty$
c	Chord length
D	Characteristic dimension - hole diameter or model base diameter
d_s	Sting diameter near the base of the model
f	Frequency
h	Height above ground
h_{HIRT}	Characteristic dimension of full-scale tunnel - test section height
h_{Pilot}	Characteristic dimension of HIRT Pilot tunnel - test section height

ℓ	Characteristic dimension over which flow must respond
M	Mach number
$\overline{M}_p$	Average plenum chamber Mach number (from plenum pressures)
$\overline{M}_{TS}$	Average test section Mach number (from centerline static pipe)
p	Static pressure
$\bar{p}$	Root-mean-square fluctuating pressure
p_B	Model base pressure
p_L	Local pressure
p_o	Stagnation pressure
p_P	Plenum chamber static pressure
q	Dynamic pressure
Re_c	Length Reynolds number based on chord length, Re/ft x c
Re_D	Length Reynolds number based on model base diameter, Re/ft x D
Re/ft	Unit Reynolds number, $\rho_\infty U_\infty/\mu_\infty$
$Re\Delta x$	Length Reynolds number based on distance to head of unsteady wave, Re/ft x Δx
r	Radial distance from exhaust stack
S_b	Model base area
T	Nondimensional flow response time, Thompson number, $t_r U/\ell$
t	Time
t_r	Flow response time
U	Local flow velocity
U_{4a}	Local flow velocity behind unsteady wave
U_e	Local flow velocity at boundary-layer edge
U_W	Velocity through the porous wall
V_P	Plenum chamber volume
V_T	Test section volume

$\dot{W}_{1a}$	Flow rate through porous test section wall
$\dot{W}_{1b}$	Flow rate through plenum exhaust system
$\dot{W}_2$	Flow rate out of charge tube
$\dot{W}_T$	Flow rate through main starting device
x	Axial dimension on body or in test section
Y	Vertical height from wall
Z	Spanwise dimension
α	Angle of attack
ΔC_D	Difference between total drag coefficient at any Mach number and coefficient at some reference Mach number
ΔC_{DF}	Difference between forebody drag coefficient at any Mach number and coefficient at some reference Mach number
ΔC_p	Fluctuating pressure coefficient, $\bar{p}/q_\infty$
Δt_P	Time between opening of main starting device and opening of plenum exhaust diaphragm
ΔW	Length between head and tail of unsteady wave
Δx	Length from measurement station to head of unsteady wave
δ	Boundary-layer total thickness
δ^*	Boundary-layer displacement thickness
η	Nondimensional semispan location, $Z/(b/2)$
θ	Angular position relative to tunnel axis in the ground plane
μ	Viscosity
ρ	Density
$\sigma\Delta M$	Standard deviation in test section axial Mach number distribution
τ	Time during run, since passage of the head of the unsteady wave, at which thickness measured
τ_W	Test section wall porosity

SUBSCRIPTS

4	Charge tube storage condition
∞	Free-stream conditions

SECTION I
INTRODUCTION

The trends in the design of large transport aircraft and high performance military aircraft have prompted an assessment of transonic wind tunnel facilities in the United States and Europe. Also, there are concerns about the adequacy of wind tunnel tests because results from flight tests are inconsistent, in some cases, with predictions based on ground-based facility data. The AGARD conference on facilities and techniques for aerodynamic testing at transonic speeds and high Reynolds numbers (Ref. 1) produced an excellent review of the current status of transonic wind tunnels and their shortcomings, Reynolds-number-sensitive flow phenomena and methods for achieving high Reynolds numbers in ground-based facilities.

The need for a high Reynolds number transonic tunnel in the United States was recognized in 1966, and studies were begun at the Air Force Arnold Engineering Development Center (AEDC) in 1967 to define testing requirements and a facility concept. Several facility types were examined, and a transonic tunnel with a Ludwieg-tube-type air storage system emerged as the most promising candidate because of high quality flow, comparatively low cost, and relatively high data productivity. A schematic drawing and artist's view of the proposed AEDC high Reynolds number transonic tunnel (HIRT) are shown in Fig. 1.

About 15 Ludwieg tube tunnels exist in the United States and Europe covering a Mach number range from 0.1 to 12 and test section size ranging from 0.022 to 5.5 sq ft. The largest of these tunnels is at the NASA-Marshall Space Flight Center (MSFC), where a 32-in.-diam tunnel has been in operation since early 1970 at Mach numbers 0.2 to 2 using a 390-ft-long supply tube. Force and pressure measurements have been obtained in this facility in a steady flow time of 350 to 450 msec at transonic speeds. The Ludwieg tube tunnels have reached an advanced state of refinement and are now producing high quality force, pressure, and heat-transfer measurements.

In support of the development of the AEDC HIRT, research has been conducted to obtain information on the flow quality and boundary-layer growth in the charge tube, effectiveness of the contraction section design, influence of plenum chamber volume, flow quality in the test section, start time of the tunnel and flow response over a moving model, concepts of start value, details of instrumentation,

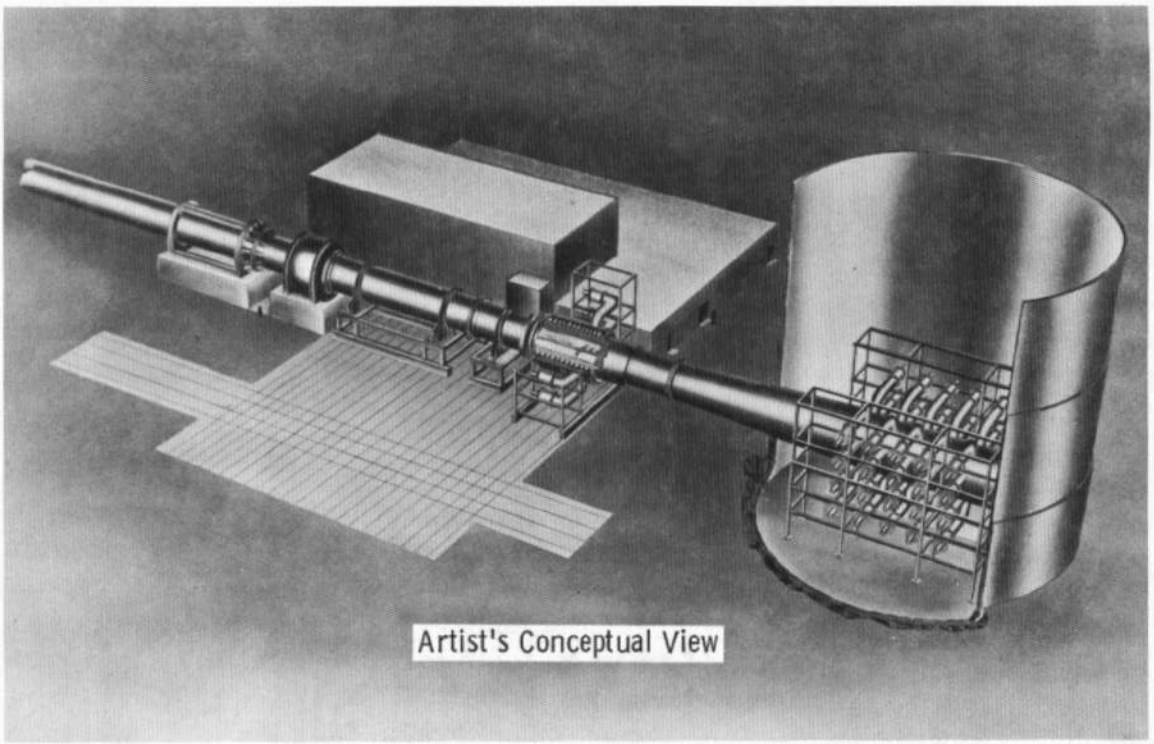

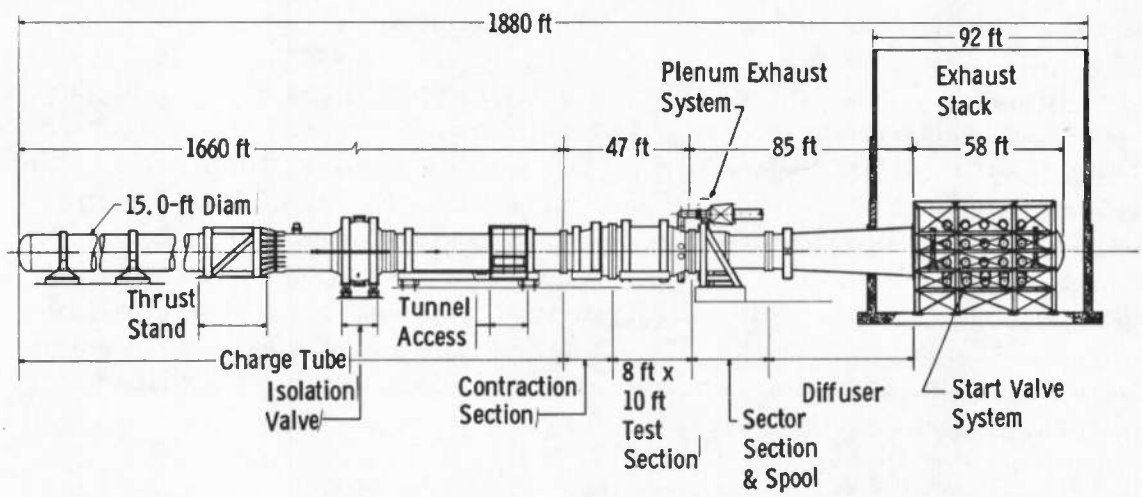

Fig. 1 General Configuration of AEDC High Reynolds Number Tunnel (HIRT)

and production of acoustic noise by the tunnel exhaust. These areas of research and numerous others have been studied since 1969 with the aid of a 1/13-scale pilot model of the major components of the full-scale tunnel, including the exhaust system. The significant results of the research at AEDC in the development of the HIRT are presented.

SECTION II
EXPERIMENTAL STUDIES IN PILOT HIRT

2.1 DESCRIPTION OF PILOT TRANSONIC TUNNEL AND INSTRUMENTATION

A schematic drawing of the pilot tunnel is given in Fig. 2. It can be charged to 800 psia and can produce a maximum stagnation pressure of about 500 psia in the transonic speed range. The Ludwieg tube storage system (charge tube) is one foot in diameter and was about 60 ft long for early tests; the charge tube was later extended to a length of 80 ft. Results from both configurations will be presented. A transition section with a 1.6 contraction ratio channels the flow from the circular charge tube into a rectangular test section which is 7.3 by 9.15 in. In the test section-plenum chamber, shown in Fig. 3, the porous walls are of conventional design with 60-deg inclined holes. The porosity can be varied manually by moving one porous plate relative to another (two plates constitute a wall) (Ref. 2). When the holes are fully aligned, the porosity is 10 percent. The plenum chamber which encloses the test section has a volume which is about 1.8 times the test section volume (neglecting the volume of the wall support structure). The plenum is exhausted directly to atmosphere through the choked orifice-valve system shown in Fig. 4. The desired flow rate through the plenum system is obtained by adjusting the orifice and by opening or closing the quick-acting valve shown in the figure. A model support section and main starting device are located downstream of the test section (Fig. 2). Both a diaphragm and fast-acting valve have been used as the main starting device in the tests which will be described. All of the exhaust air is channeled out of the building through the main exhaust system.

The tunnel run is initiated by opening the main starting device and the plenum exhaust system. The duration of the first cycle of the blow time of this pilot tunnel is 105 or 135 msec, depending on the charge tube length. The duration of the steady portion of the run will be discussed later.

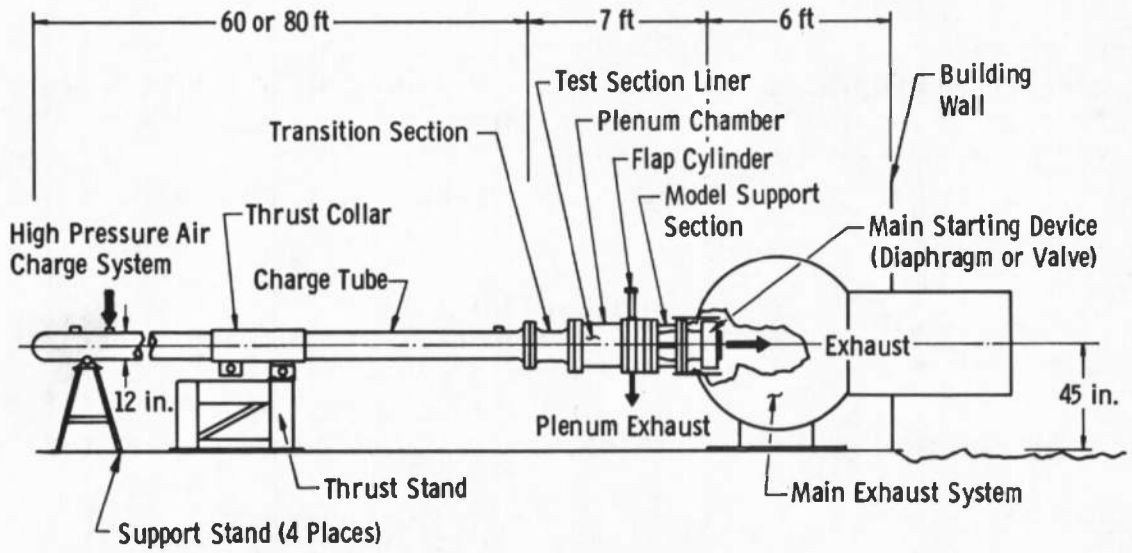

Fig. 2 Pilot HIRT Schematic

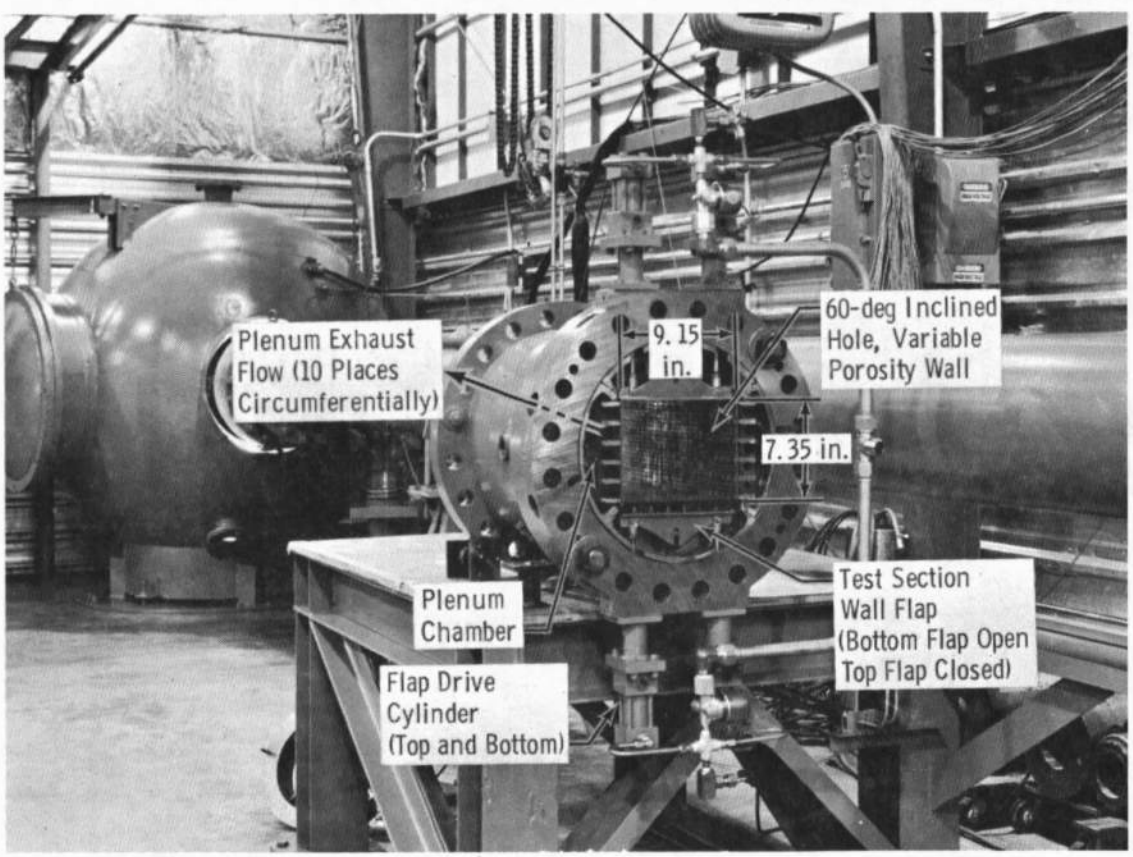

Fig. 3 Pilot HIRT Test Section—Plenum

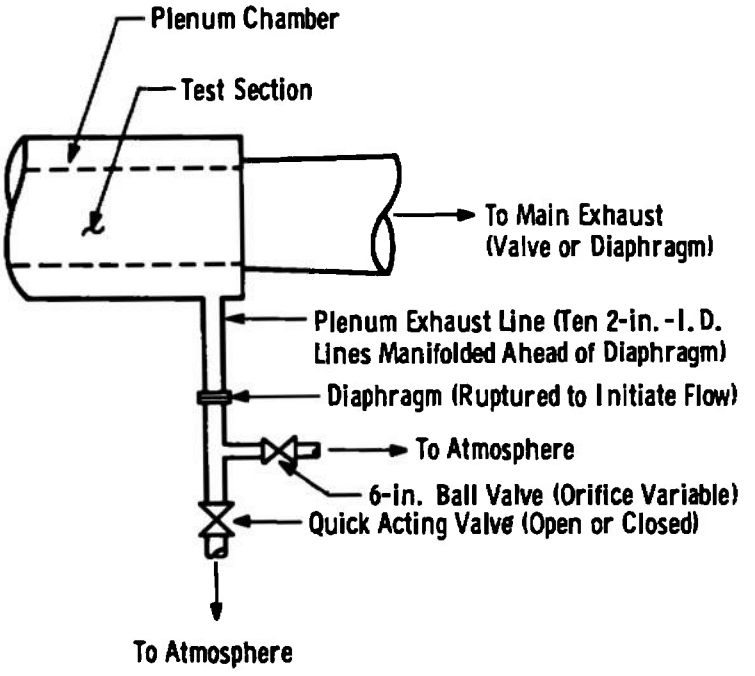

Fig. 4 Schematic of Plenum Exhaust System

To date, timewise variations and accurate steady-state values of pressure and force have been measured. Individual pressure transducers are used for each channel. Both strain-gaged diaphragm units built at AEDC-VKF and commercially available Tabor® transducers are employed, depending on the frequency response desired in the pressure measurement. A rapid-response, three-component load-cell-type balance has been used for the force measurements. The two normal-force and one drag-force load cells are instrumented with semiconductor strain gages. The balance is 1/2 in. in diameter and 3 in. long.

Two systems have been used to record the pressure and force signals in these experiments. Transient measurements in the starting process or high frequency fluctuating pressure measurements are recorded on an oscillograph or oscilloscopes. Because of reading errors associated with taking data from these types of recorders, more accurate steady-state measurements are recorded with a digital voltmeter which has a printer readout. The scan rate of the particular system used in this study is relatively slow (about 3 to 10 samples per second), and a one-time point trapping system is used to hold the steady-state run reading until it can be recorded by the scanner-digital voltmeter after the tunnel run is actually completed. A fast-acting

pneumatic trap valve or an electrical "track and hold" network has been used with equal success to accomplish this. These two systems are shown schematically in Fig. 5.

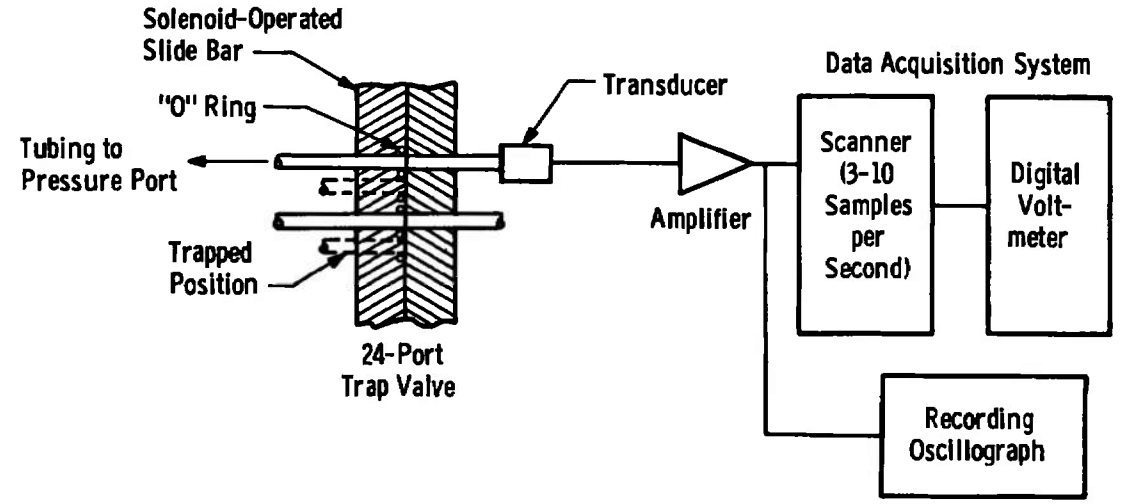

a. Trap-Volume System

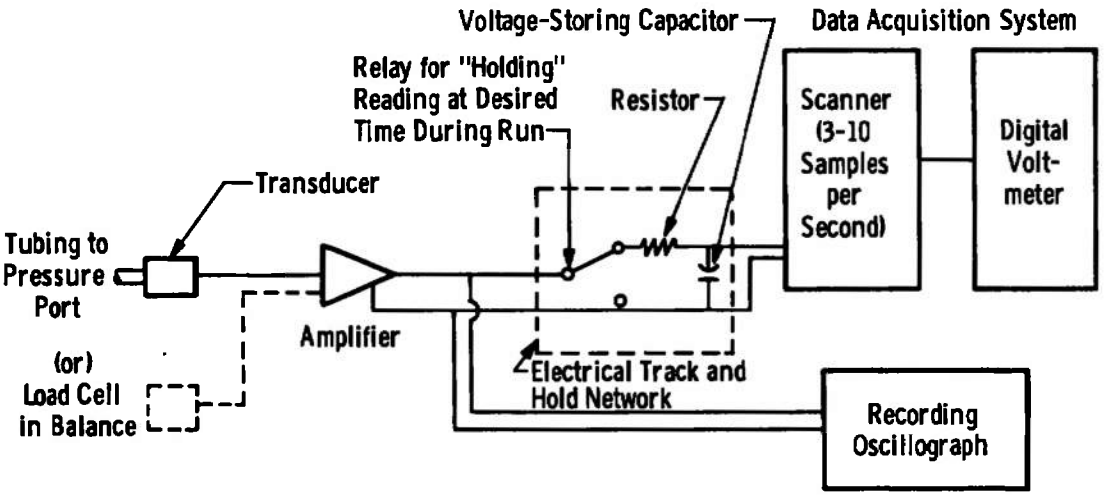

b. Electrical Track-Hold System

Fig. 5 Pilot HIRT Data Recording Systems

To adequately study the starting process or noise levels in the test section, the transducers must be mounted with the diaphragm at the point of measurement in the tunnel. The lag or ring produced by any length of tubing cannot be tolerated. The small AEDC-built transducers are mounted on the tunnel wall, tunnel centerline, or directly in the model for these measurements. For steady-state measurements, the transducers have been located outside the tunnel because of the bulk of the trap valve required in the system in some cases or ease of system maintenance in other cases. Care has been taken to obtain data of the required accuracy through the approximately 4-ft tube lengths that result. The length of all tubes has been held nearly constant to minimize length-induced variations in response. The response of a tube does vary; however, with pressure. A tube of a given length which has a damped response on a low pressure run (charge pressure $\approx$ 70 psia) has an underdamped response (ring) at higher pressure (charge pressure > 200 psia). The amplitude of the ring increases with pressure. Wire coils have been inserted in the tubes to minimize the amplitude or ring at some sacrifice to response. As a rule, both transient and steady-state measurements are made simultaneously in a run.

Both the high frequency response of the oscillograph and the accuracy of the trap technique are available in single state-of-the-art multiplexing-analog-to-digital conversion systems which provide digitized results in real time. The availability of such an improved system eliminates the necessity of using the multiple recording techniques with the complexities just described.

2.2 TUNNEL STARTING PROCESS AND TIME

A critical area of study involves the starting wave process and start time of the tunnel. The required high quality transonic measurements can be made only if tunnel conditions are constant for the duration of the useful run and if the steady conditions are established spatially throughout the test section. In relation to the full-scale HIRT, it is also important to minimize the start time in order to maximize the duration of steady-state conditions for a fixed Ludwieg tube length; the productivity of data will depend on the number of angle-of-attack points which can be obtained during each run.

After the main starting device (diaphragm or valve) is opened, the unsteady wave which moves through the test section into the charge tube cannot come to an equilibrium strength i. e., - establish steady flow out

of the charge tube - until flow through the plenum chamber which surrounds the test section has reached an equilibrium value. This does not occur until the plenum chamber pressure adjusts from the high value at charge to a level slightly less than the test section free-stream static pressure. The process is illustrated schematically in Fig. 6. When the main starting device opens, the total flow rate ($\dot{W}_T$) consists of the combined flow rates entering the test section from the plenum ($\dot{W}_{1a}$) and the charge tube ($\dot{W}_2$). As the plenum pressure drops and the pressure ratio across the porous wall decreases, the flow rate from the plenum chamber into the test section decreases; and the flow rate out of the charge tube must increase to maintain the nearly fixed total flow rate ($\dot{W}_T$). Eventually, the flow rate through the porous wall reverses direction, and equilibrium is reached when the flow rate into and out of the plenum becomes equal ($\dot{W}_{1a} = \dot{W}_{1b}$). At this time, the flow rate out of the charge tube maximizes and the starting process is completed. From this description of the starting process, it can be seen that increasing the flow rate out of the plenum chamber ($\dot{W}_{1a}$ and $\dot{W}_{1b}$) during the tunnel start can have a marked effect on the starting time.

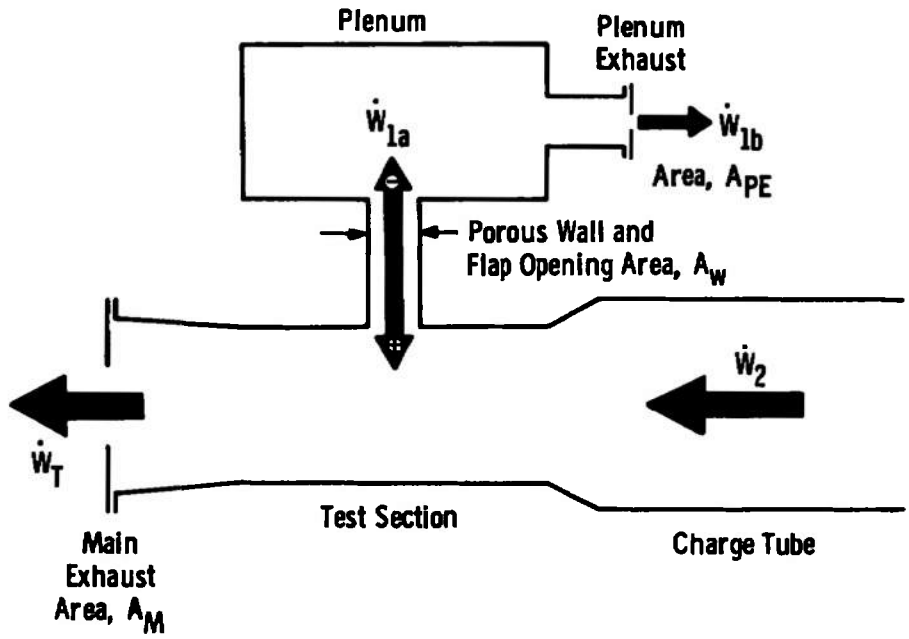

Fig. 6 Schematic Illustration of Flow Process during Tunnel Start

In the pilot tunnel, three devices are provided to facilitate fast tunnel starts:

1. A plenum exhaust which can be opened independently from the main tunnel exhaust;

2. A controllable plenum exhaust system which can provide an excessive plenum exhaust flow during the starting process and be throttled to the lower exhaust flow required during the steady run; and

3. A flap system in the tunnel wall which can be opened to increase the flow area between the test section and plenum chamber during the tunnel start.

It was felt that the independent plenum exhaust would offer the alternative of partially pumping the plenum prior to establishing the main tunnel flow. However, as illustrated in Fig. 7, the small unsteady wave which travels up the charge tube if the plenum is opened early reflects and prematurely ends the run. Likewise, if the plenum exhaust is established after the main tunnel flow, the useful run duration is reduced. The experimental data which illustrate this are plotted in Fig. 8 for $M_\infty = 0.75$. It is concluded that the sequence of opening the plenum exhaust and main tunnel exhaust should cause the expansion wave from each to reach the test section simultaneously. In this way, no disturbances are generated until "useful" pumping of the plenum is initiated, and pressure adjustments across both expansions occur at the same time. Unless there is a significant difference in the distance of each starting device from the test section, these data indicate that the two flows should be established simultaneously.

Experimental results have shown a more pronounced influence of the controllable plenum exhaust mode of operation on the tunnel start time. The tunnel start time can be significantly reduced by employing the excess plenum exhaust as needed in the start. This is shown in Fig. 9 (Ref. 3) which illustrates the variation in test section static pressure with time. Note that the start time with excess exhaust was reduced to one-half the value without excess exhaust. Because of restrictions in the pilot tunnel plenum exhaust flow system (which limits the auxiliary flow rate to a maximum of about 12 percent), only test conditions at about Mach 1.0 or less can be achieved with a sufficient excess flow.

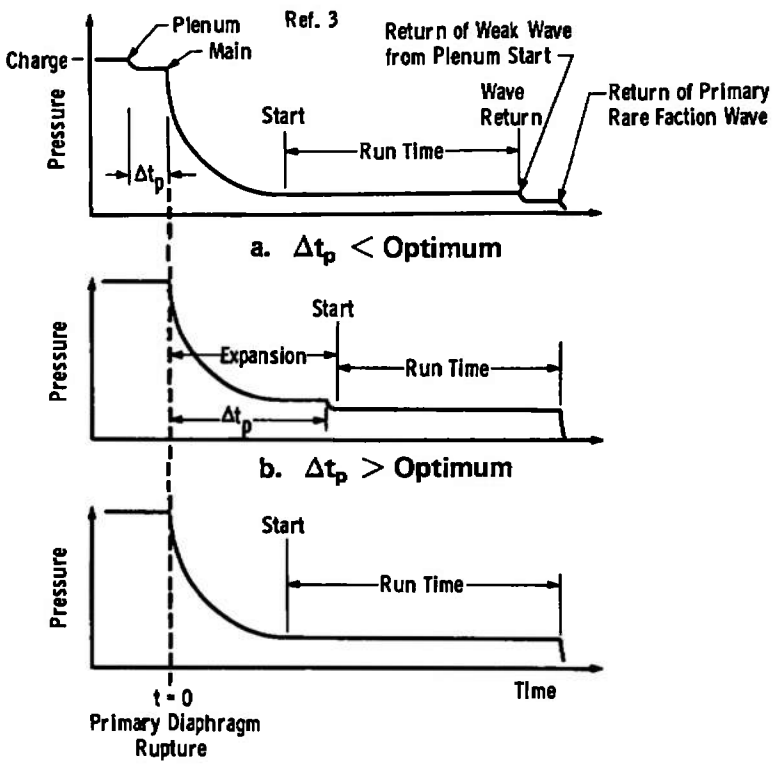

Fig. 7 Schematic Representation of Timewise Pressure Variation in the Test Section

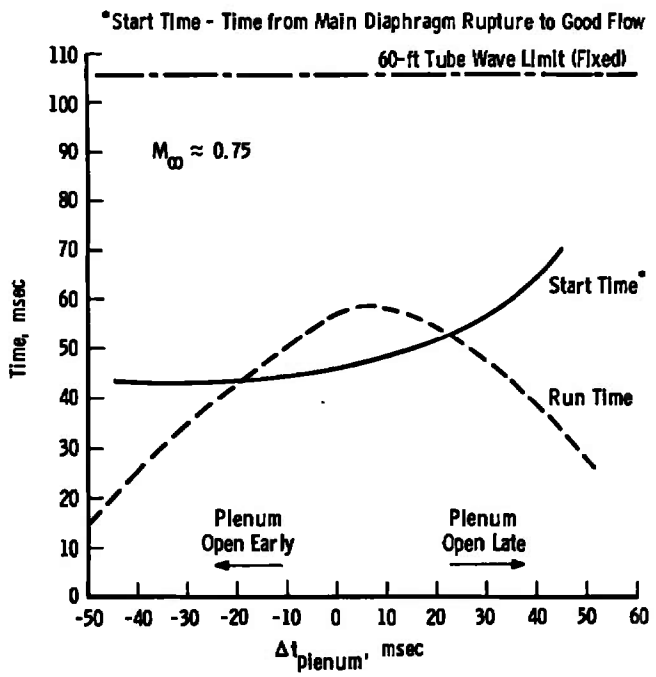

Fig. 8 Start and Run Times in the Pilot Tunnel for Various Plenum Delays

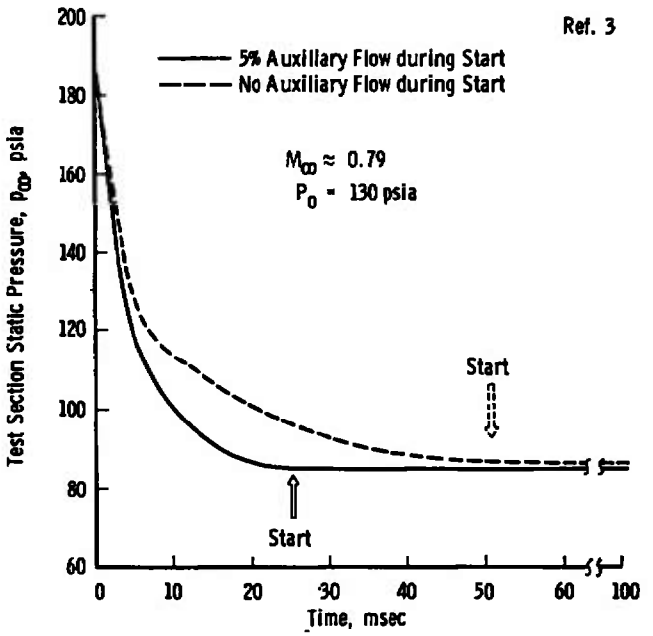

Fig. 9 Influence of Utilization of Excess Plenum Flow during the Starting Process

The variation of tunnel start time with free-stream Mach number is given in Fig. 10. If the pilot tunnel is operated along the solid curve to the right of the figure - that is, without excess plenum exhaust during the start - the start times are rather long. In fact, the tunnel does not start, technically, above Mach ≈ 0.95 before the reflected wave ends the run. Mach numbers as high as 1.25 have been achieved, but a slight gradient in pressure is still evident in the test section when the run ends. It takes all of the plenum exhaust available in the pilot tunnel to reach this Mach number, and no significant excess is available to use during the start for Mach numbers above about 1.0.

If the tunnel Mach number is reduced below the maximum, a reasonable excess is available for starting. With 5-percent excess, the tunnel starts in approximately one-half the time at $M_\infty = 0.8$, as shown in Fig. 10. This particular data point was shown in another form in Fig. 9. Based on these limited data points, and some judgment, the dashed curves have been faired in to indicate expected trends. It should be noted that a start can be achieved only in the pilot facility at Mach numbers above 1 by using the excess plenum exhaust. Some 8- to 10-percent excess exhaust will be required to start the pilot tunnel in a short time at Mach 1.2. This means that at least 20-percent

plenum exhaust must be available since approximately 10-percent plenum weight flow is required for steady-state flow at Mach 1.2.

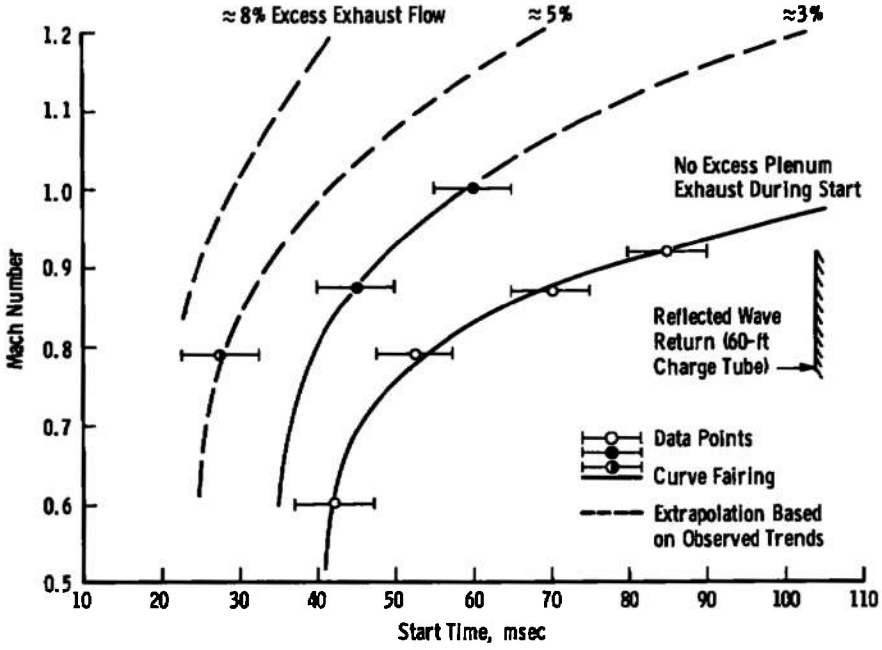

Fig. 10 Pilot HIRT Start Times for Various Excess Plenum Flow Rates during the Start

The test section flaps located at the downstream end of the test section in the top and bottom walls (see Figs. 3 and 11) are intended to provide a large open area between the test section and plenum chamber during the start. Tests to date have been conducted with 4- and 6-percent wall porosity settings only, and no noticeable influence of the flaps on the start time has been seen. Certain test conditions in transonic tunnels, however, require that the wall porosity setting be significantly less than four percent. For such cases, the influence of the flaps in providing a large flow rate across the test section wall during the start should be more pronounced.

Since the pilot tunnel is an exact scale version of the proposed full-scale HIRT, these start time results can be used to predict start times in the full-sized tunnel. A simple dimensional ratio (h_{HIRT}/h_{Pilot} = 13) indicates that the start time of a Ludwieg tube with an 8- x 10-ft test section and a plenum volume of about 1.8 times the test section

volume and an excess exhaust of about 8 percent will be less than 0.4 sec at Mach 0.8 and under 0.7 sec at Mach 1.2. For HIRT, this predicts a useful, steady-state run time of 2.3 to 2.6 sec. The validity of a simple dimensional ratio in scaling these pilot data has been verified through both an analog and a digital solution of the starting flow process.

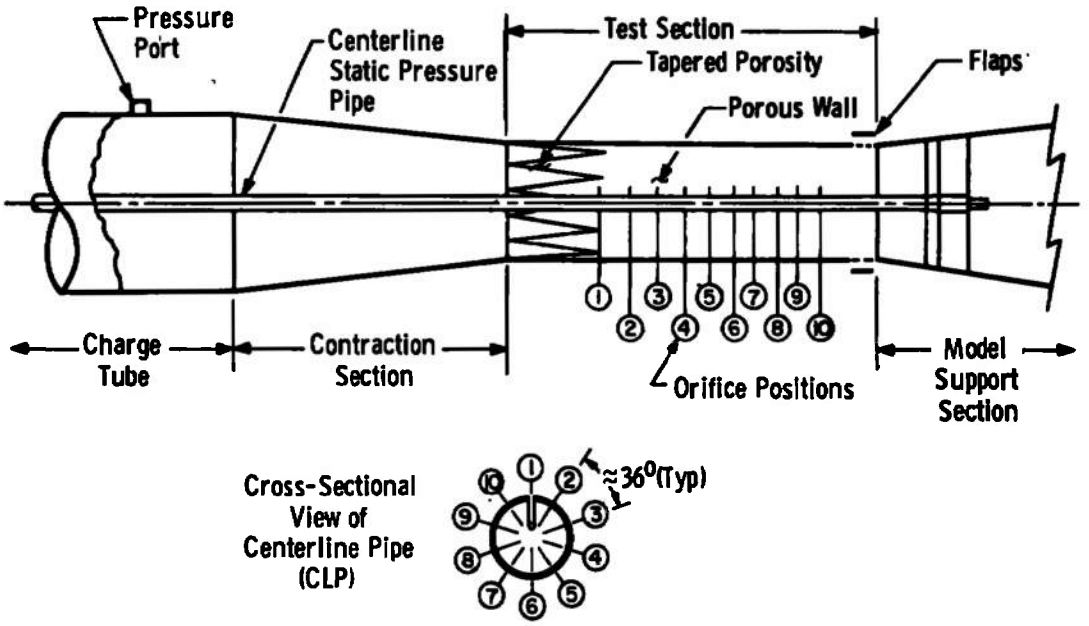

Fig. 11 Sketch of Test Section with Centerline Pipe Installed

2.3 TEST SECTION FLOW UNIFORMITY

2.3.1 Test Section Flow Uniformity–Spatial Mach Number Distributions

The axial uniformity of Mach number is a prime measurement of test section flow quality in transonic tunnels. A centerline pressure pipe (Fig. 11) with 10 static orifices was used in the pilot tunnel to make this measurement. The blockage of this static pipe is 0.6 percent.

Repeated centerline static pressure calibrations of the Pilot HIRT test section have been made in the course of this research. Each time, some improvement was made in the instrumentation and pressure system to provide more accurate data. The current axial Mach number

distribution is given in Fig. 12 for three charge pressures. Data from positions 3 and 4 have been omitted because of an erroneous measurement produced by orifice irregularities. The axial distribution was essentially the same for all charge pressures and Mach numbers tested. Additional data taken at higher charge pressures with a less precise experimental setup are presented in Ref. 3. The Mach number deviation illustrated in Fig. 13 is consistently within the band reported in Ref. 4 for all conditions. These data on the spatial uniformity of the test section flow, along with the starting results of Section IIb, certainly indicate the absence of any unexpected unsteady flow processes.

During these runs, several plenum pressures were measured to determine the relationship between the test section and plenum Mach numbers. This relationship is given in Fig. 14, and the trend with Mach number is consistent with the data of Ref. 4 for the wall porosities tested.

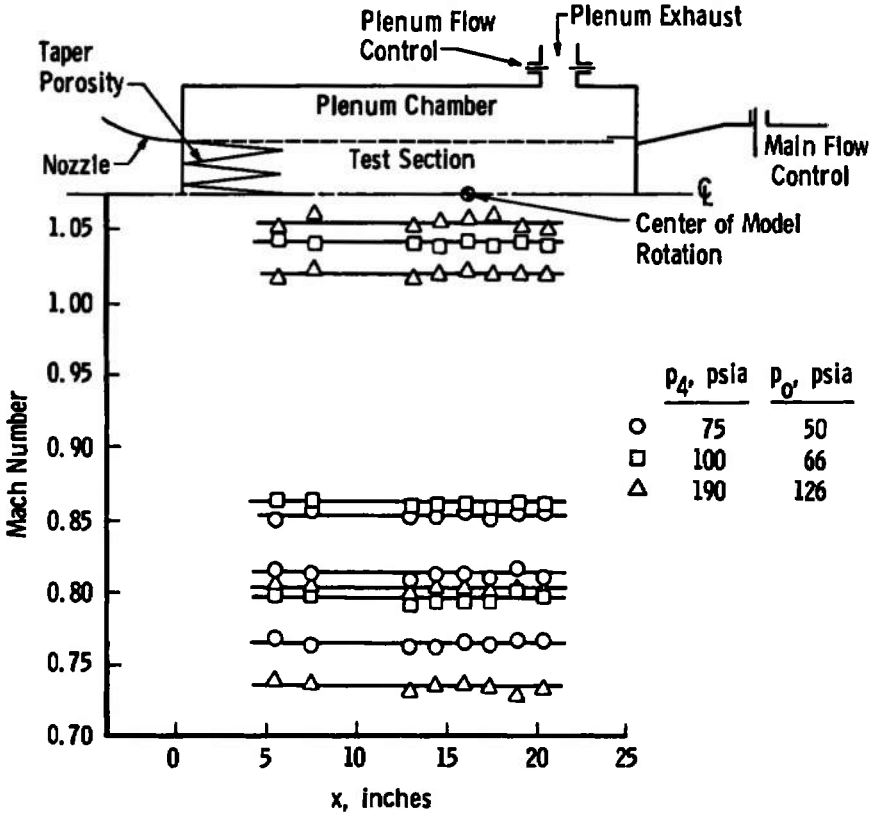

Fig. 12 Mach Number Distributions for Various Charge Pressures

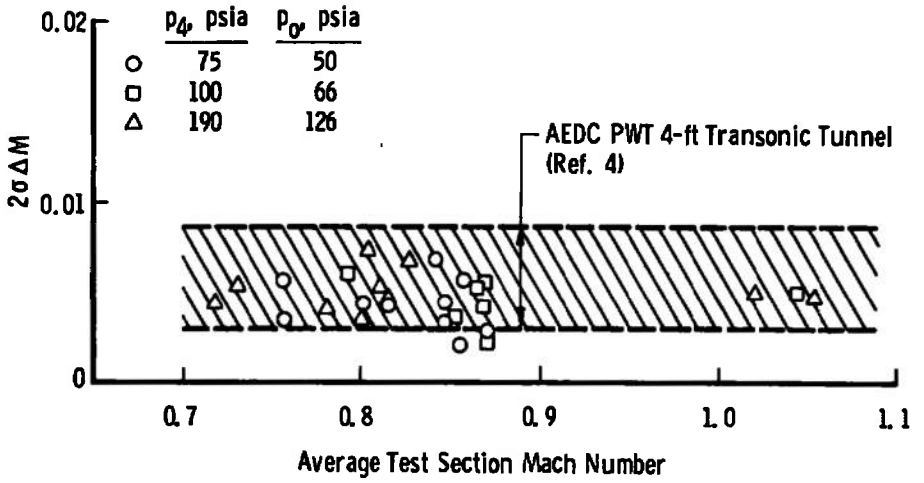

Fig. 13 Standard Deviation of Test Section Mach Number in Pilot HIRT

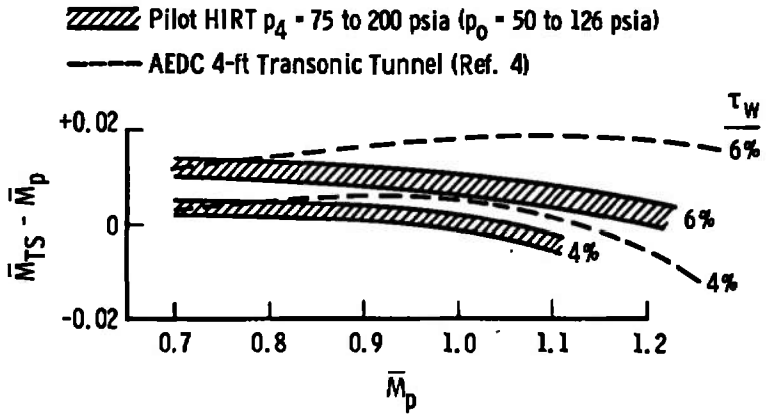

Fig. 14 Plenum-Test Section Mach Number Relationship

2.3.2 Test Section Flow Uniformity—Pressure Fluctuations

Sources of disturbance which cause fluctuations or timewise variations in flow pressure exist in all wind tunnels. Measurements of these pressure fluctuations have been made in conventional transonic tunnels (Refs. 5, 6, and 7). Similar measurements were made in Pilot HIRT for comparison with those of the more conventional transonic tunnels and to provide a further indication of the flow quality available from a short-duration facility.

There are three items of interest regarding these fluctuating pressure measurements:

1. The root-mean-square (rms) value of the fluctuating component of pressure - i.e., the severity of the fluctuation relative to the steady-state static pressure;
2. The frequency content of the fluctuation, with its implications on obtaining data in a short-duration tunnel; and
3. The source and mechanism of the pressure disturbance - i.e., the potential for reducing the noise.

The first item can be determined rather accurately from the data taken in the pilot tunnel, the second item is more difficult but can be established within limitations, and the third item is still under investigation in many transonic tunnels.

The very short duration of the run and the high pressures involved make it difficult to employ conventional noise recording techniques. As a result, AEDC-built strain-gaged diaphragm transducers with natural frequencies of 50,000 to 100,000 Hz were used as microphones. The data were recorded on tape and studied on a Spectral Dynamics analyzer. The acoustic transducers were mounted on a 10-deg cone located near the center of model rotation in the test section. Special attention has been given in the analysis of selected runs between Mach 0.5 and 1.1 which were made with a wall porosity setting of 4 percent and are typical of all runs made in the acoustic test. Oscilloscope traces from a typical run are shown in Fig. 15 (Ref. 3). These represent a 4-msec sample of the fluctuations in pressure out of the 50 msec of data taken on the recorder. Despite the limited sample, the analyzer data show a consistent run-to-run spectral content.

The rms pressure fluctuation is presented in a coefficient form and is compared with data from several continuous transonic facilities in Fig. 16. Even though the pressure level in Pilot HIRT is signifl-cantly above that of existing tunnels, the percentage of fluctuation in the free-stream static pressure is the same as or below the levels in existing tunnels ($\tilde{p}/p \lesssim 1$ percent, $\Delta C_p/q \lesssim 2$ percent). The frequency distribution of this pilot tunnel noise is given in terms of a power spectral density in Fig. 17. A large portion of the power is present in the 4- to 6.5-kHz range with additional peaks at 8 to 9 kHz and 11 to 15 kHz. The power below 3 kHz has been shown to be mechanically induced during this test in a manner similar to that described in Ref. 3.

Ref. 3

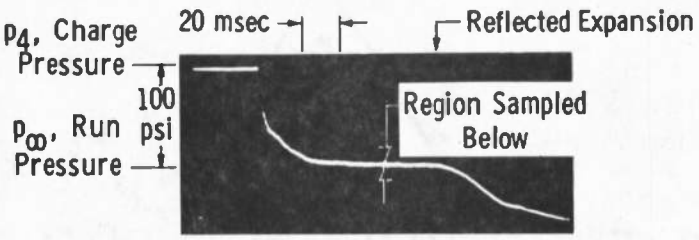

a. Typical Pressure Variation with Time

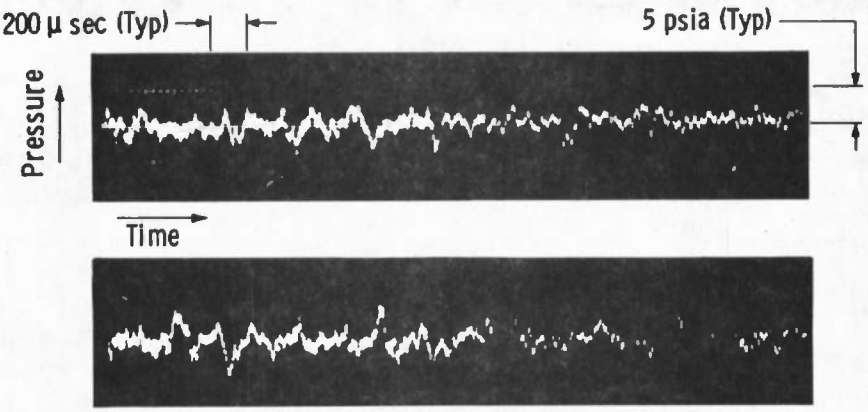

b. Pressure Fluctuation, $M_\infty \approx 0.87$

Fig. 15 Pilot HIRT Free-Stream Pressure Fluctuations

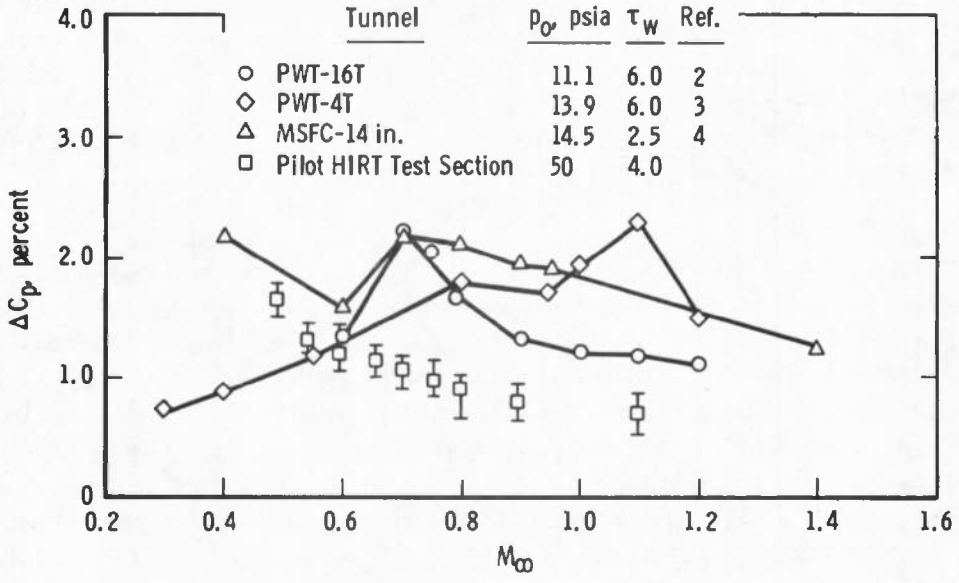

Fig. 16 Comparison of Fluctuating Pressures in the Test Section of Transonic Tunnels—Measured on 10-deg Semi-Angle Cone

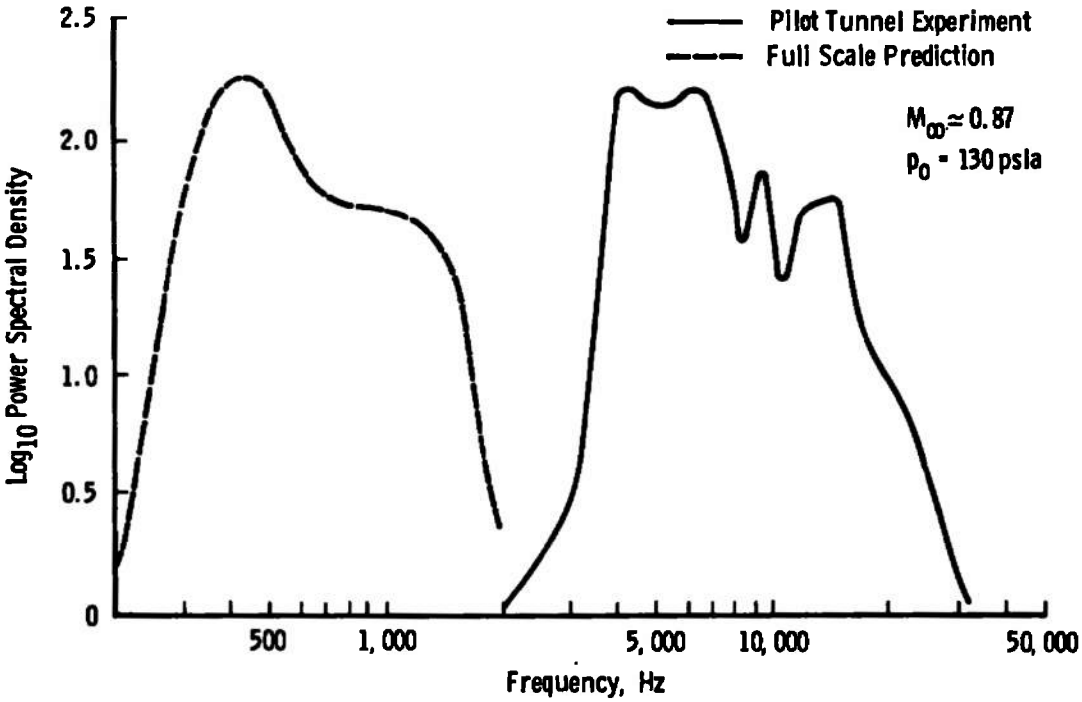

Fig. 17 Frequency Distribution of Pilot HIRT Test Section Noise and Full-Scale Prediction

If the source of the noise is viewed as a purely jet noise phenomenon, the frequency can be correlated by the Strouhal number. The peak frequency in the jet occurs at a Strouhal number, fD/U, of 0.25. The following discussion is intended to analyze the parameters which should be used to scale these pilot data to the full-scale HIRT. In Pilot HIRT, the diameter of the hole through the test section wall is 0.12 in. for the maximum porosity. At a porosity setting of 4 percent, the opening corresponds to a diameter of about 0.07 in. To estimate the flow velocity through the walls, continuity of flow and the plenum exhaust rate can be used. For 8-percent auxiliary flow at Mach ≈ 0.87 with a 4-percent wall setting, the velocity is approximately 170 fps. This is only an average velocity through the wall, however, and greater or lesser local velocities can be expected, depending on the crossflow requirements to maintain a uniform axial condition in the test section. The predominant frequencies present in the spectral analysis could conceivably come from jet flow through the walls. The large power at 4 to 6.5 kHz, in fact, corresponds to the major jet diameter of ≈0.12 in. and a velocity of ≈200 fps.

A sample of the variable-porosity wall has been tested to verify this conclusion. The wall sample was mounted in a baffled, acoustically treated box. Flow was established through the holes at velocities

approximating those in the actual test section (without any mean flow across the plate). The box was connected to a vacuum tank and flow controlled through the wall sample by means of a metering orifice. Run times were long and pressures were low enough that conventional microphones and noise recording equipment could be used. Flow velocities of ≈100 to ≈400 fps in the holes were tested. The purpose of the test was to determine if the noise produced by flow through the wall behaved in a manner predicted by jet noise theory and if the frequencies found in the tunnel could be duplicated.

The data obtained with the acoustic sample box are shown in Fig. 18 for the full range of wall velocities tested. Note that the frequencies shift as expected for an increase in velocity, i.e., an increase in velocity produces a proportionate increase in frequency, and that the frequency content is very similar to the actual test section run data. The frequencies evident in the data fall very close to those expected from the physical hole size in the wall sample based on jet noise theory. It certainly appears reasonable, judging from these considerations and other evidence of tunnel noise, that the pilot frequency spectrum should be scaled to the full-scale tunnel by the inverse of the wall hole diameter ratio. The lowest aerodynamic frequency predicted for the full-scale tunnel based on these experiments is 200 Hz with the dominant aerodynamic noise at 400 Hz (see Fig. 17). Either filtering or time-averaging can easily be applied in the full-scale data recording system to accurately handle the 1-percent rms fluctuations at these relatively high frequencies even if the duration of the flow is only 2-1/2 sec for the full-scale HIRT facility. Filtering and time-averaging are exactly the techniques currently employed to process data from wind tunnels where the experimentalist must usually contend with very low frequency fluctuations in the order of a few cycles per second.

Valid concern has been expressed about the influence of these wind tunnel flow fluctuations on the basic vehicle aerodynamics (Ref. 8). The fluctuating pressures sensed in the measurements described above have a spatial distribution in addition to the timewise variation, and they interact with the model flow field in a manner which is not clearly understood. These spatial and temporal fluctuations have been shown experimentally to induce premature boundary-layer transition to turbulence and cause sufficient variation in the flow field over the model to compromise the validity of dynamic-stability measurements among other things. These are not new wind tunnel problems, but they do gain importance when one attempts to sort out "Reynolds number effects." An obvious concern about these phenomena developed into one of the basic, fundamental criteria in the choice of the Ludwieg tube concept for a high Reynolds number transonic tunnel described in Ref. 3.

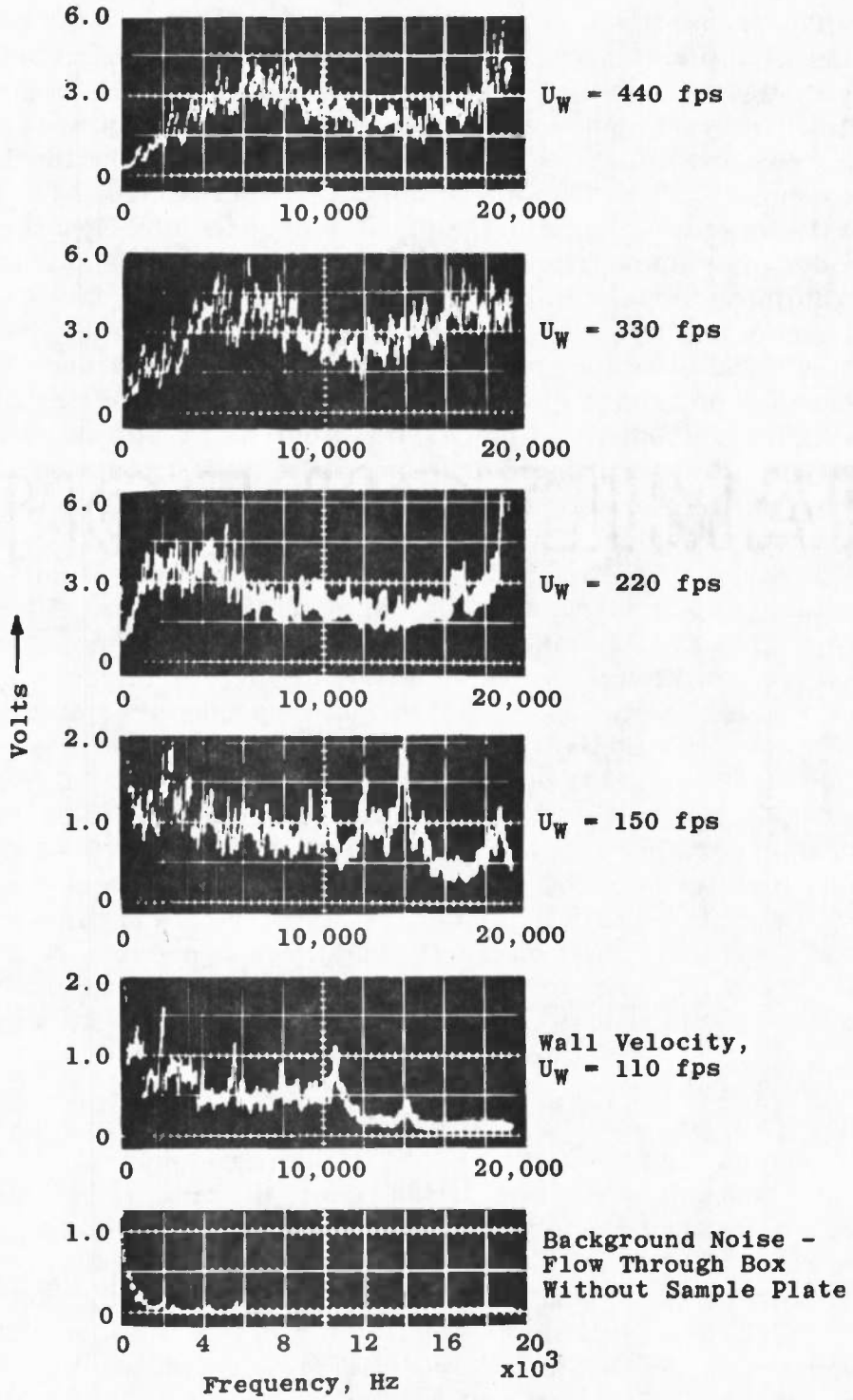

Fig. 18 Spectral Content of the Noise Produced by Flow through Wall Sample at Specified Velocities

The frequency of the noise will primarily determine its influence on the wind tunnel flow field. There is some evidence (Ref. 9) that only the lower frequency fluctuations (<100 cps) excite the overall model flow field, as shown in Fig. 19. The frequency distribution of the shock movement is very similar to the distribution of the tunnel noise up to about 50 Hz. The shock appears to be strongly excited by the flow-field fluctuations (aerodynamic noise) up to about 50 Hz; however, aerodynamic noise above 150 Hz does not cause any detectable shock oscillation. The overall flow field about the model cannot respond to, and hence will tend to be less influenced by, the higher frequency fluctuations. As already discussed, the lower frequencies which can produce the significant flow field distortion appear to be much less dominant in a Ludwieg-tube-type facility. Further basic research into the noise environment of the pilot tunnel and a determination of the proper scaling parameters is currently underway.

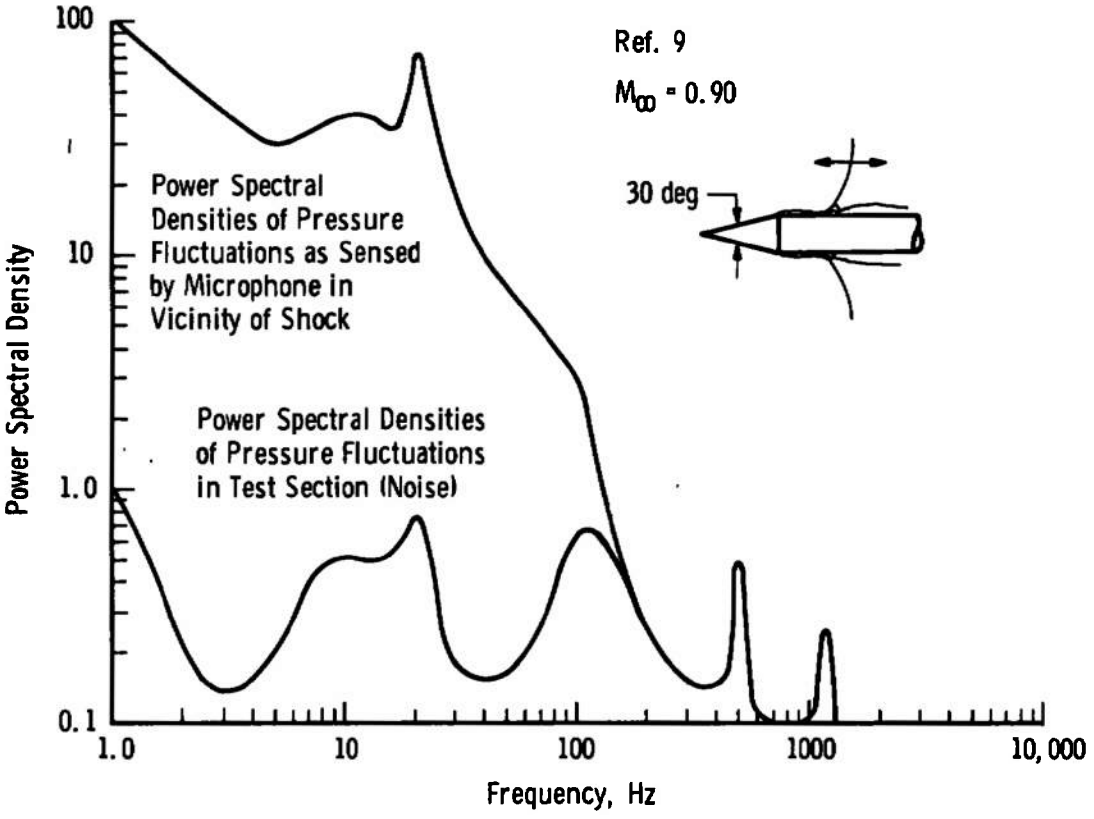

Fig. 19 Influence of Low Frequency Tunnel Flow Oscillations on Shock Movement at Shoulder of Cone-Cylinder

2.3.3 Tunnel Wall Boundary-Layer Characteristics

An understanding of the flow process in the charge tube of any Ludwieg tube tunnel is a basic requirement for properly mating the test section and storage system to minimize flow disturbance during the tunnel run. One of the sources of poor quality flow from the charge tube is the turbulent boundary layer which grows on the wall. Typical lengths of charge tubes tend to be so large that significant boundary-layer thicknesses are produced in spite of the thinning influence of very high unit Reynolds numbers. The charge tube boundary layer, of increasing thickness, can produce both radial and timewise gradients in flow properties. Since economic considerations dictate a minimum charge tube diameter for a given test section size, the implications of the charge tube boundary layer on test section flow must also be considered. A detailed theoretical treatment of this unsteady boundary-layer problem has been reported by Becker in Refs. 10 and 11. Although no explicit measurements of the boundary-layer thickness on the charge tube wall have been reported, the timewise measurements of pitot pressure shown in various Ludwieg tube reports (Refs. 12, 13, and 14) can be used to infer a boundary-layer thickness. Rather than rely completely on this comparison for the proposed full-scale HIRT, it was felt that measurements in the pilot facility were required.

Boundary-layer survey rakes were installed in the pilot tunnel at the locations shown in Fig. 20. These locations were the charge tube exit, the contraction exit, and the center of model rotation in the test section. Runs were made at charge pressures of 100 to 600 psia. The profiles were measured at a selected time point during the run and also were recorded on an oscillograph through the run.

In general, the run-to-run repeatability and agreement in the pressure measurements between all probes outside the boundary layer have been about ±1/4 to 1/2 percent (depending on the instrumentation system employed). For probes inside the boundary layer, the run-to-run repeatability was about ±1 percent. This was due to the limitations of a fixed-time-point measurement considering the fluctuating nature of a turbulent boundary layer and a slight tube ring on some of the higher pressure runs.

The boundary-layer profiles obtained at the charge tube exit with the single time-point trapping measurement system are given in Fig. 21. The profiles are shown for a given charge pressure and a range

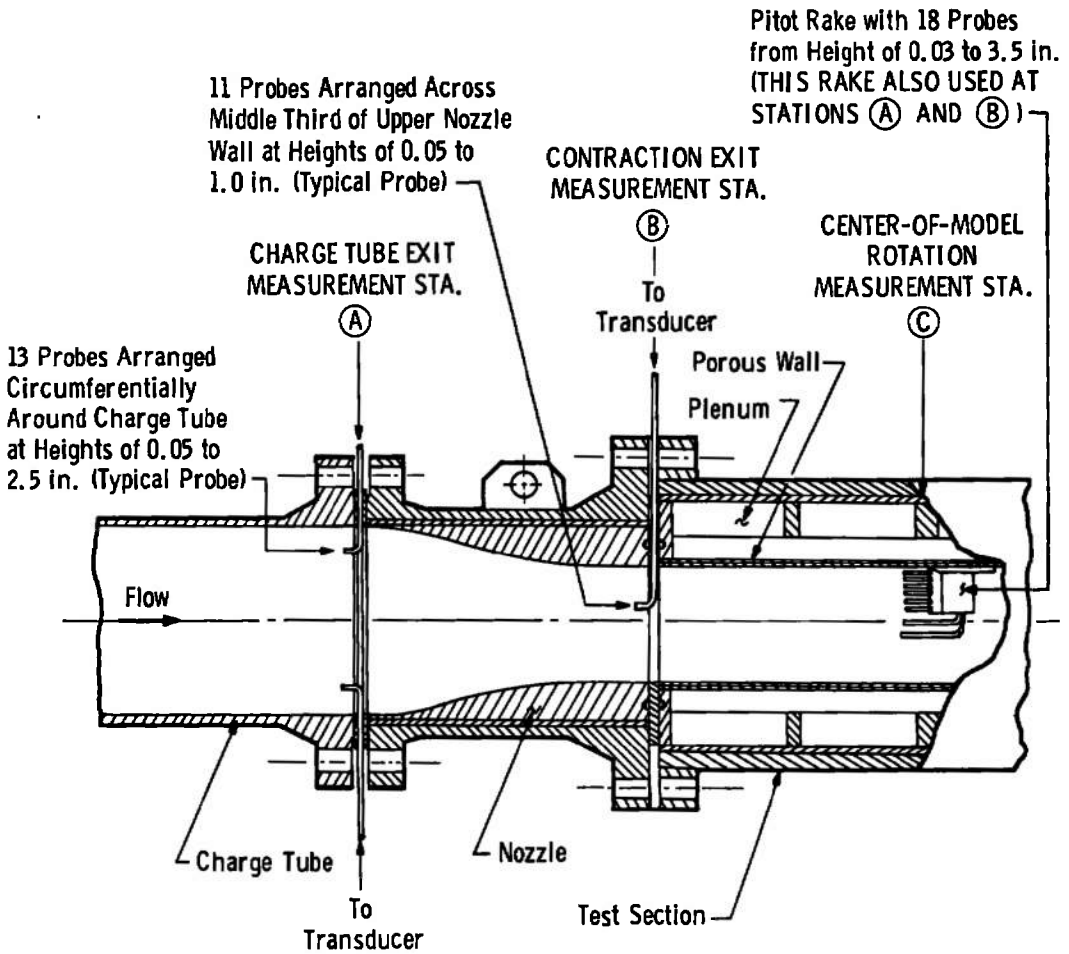

Fig. 20 Diagram Illustrating Location of Boundary-Layer Survey Rakes in Pilot HIRT

of times during the run (taken on multiple runs). The velocity distributions are fully turbulent with 1/7- to 1/9-power-law profiles, depending on the time at which the data are taken. The velocity ratio is calculated from the measured pitot pressure profile based on the assumption of an isothermal boundary layer. There is a slight heat transfer from the tunnel wall in the operation of the Ludweig tube since the stagnation temperature of the flow is lower than the charge temperature (tunnel wall temperature). Calculations have shown that the effect of this temperature variation on the velocity distribution through the boundary layer is small. The best judgement of the experimental boundary-layer edge location is shown in each case.

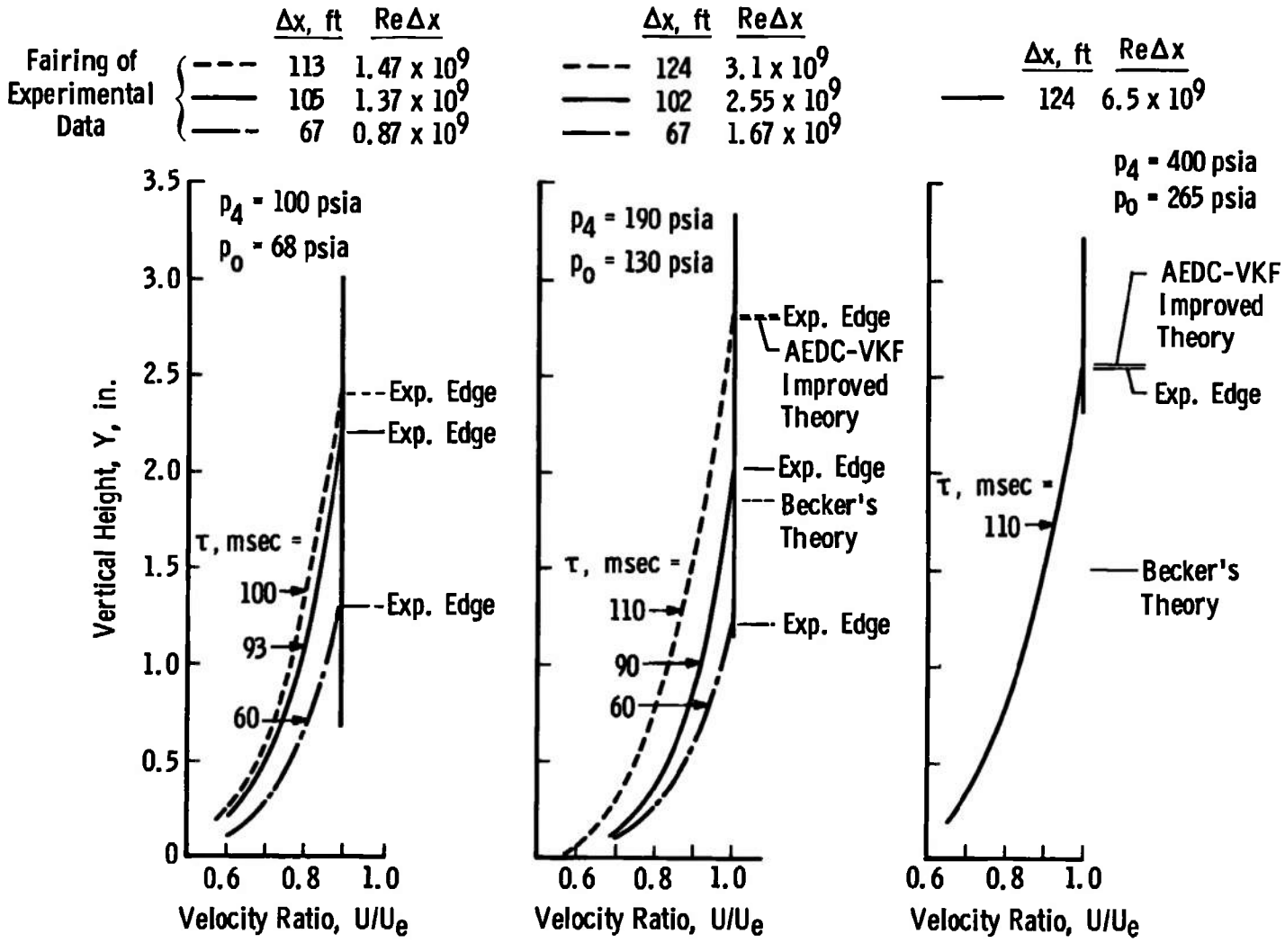

Fig. 21 Boundary-Layer Velocity Profiles at the Charge Tube Exit

A measurement of the boundary-layer thickness was also obtained from the oscillograph trace itself. As long as a given probe is outside the boundary-layer edge, it measures a constant p_o. As the boundary-layer edge grows out to, and past, the probe, the pitot pressure drops measurably. By noting the time during the run at which the pressure change is first seen at a probe of known height, an "instantaneous" boundary-layer height measurement can be made. A typical trace of this phenomenon is shown in Fig. 22. This variation in boundary-layer thickness with time was found to be in good agreement with the fixed time-point data; however, the instantaneous edge was about 20 percent thicker than mean position of the boundary edge measured with the trapping system. This is to be expected based on Fig. 23, taken from Ref. 15, which illustrates the observed phenomenon.

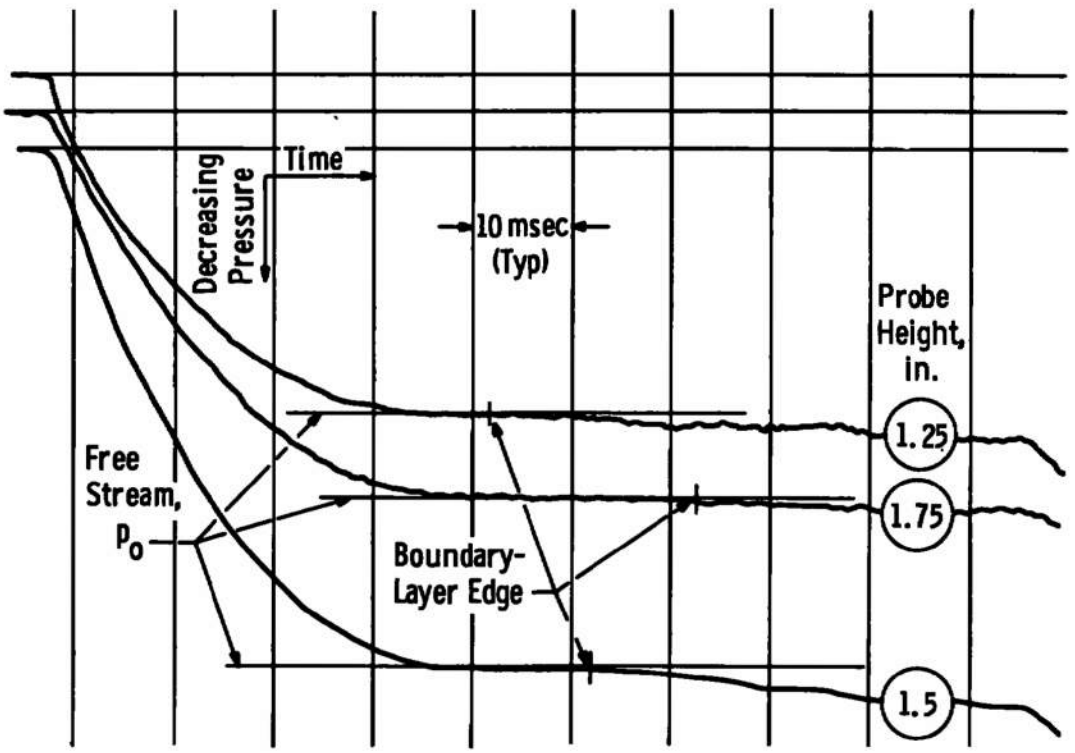

Fig. 22 Oscillograph Trace, Pressure versus Time

In relating these measurements to the theory which has been developed by Becker, a study of Fig. 24 is helpful. As the wave passes down the tube and sets the gas into motion, a boundary layer grows. The growth inside the wave is strongly influenced by the favorable pressure

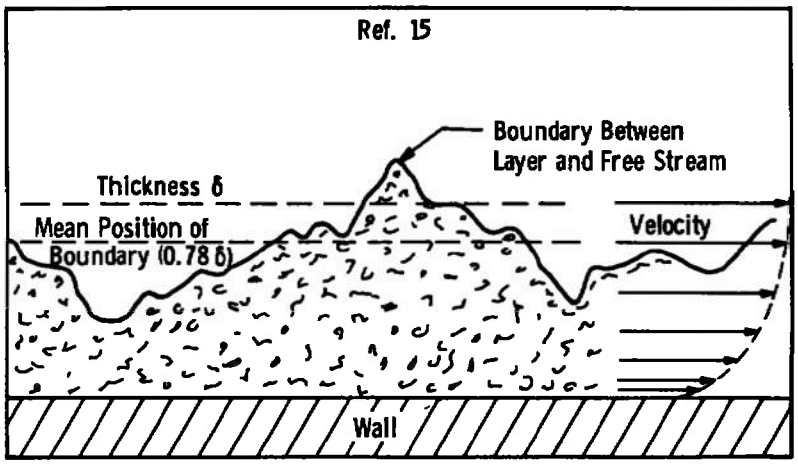

Fig. 23 Schematic Diagram of Boundary-Layer Velocity Profile

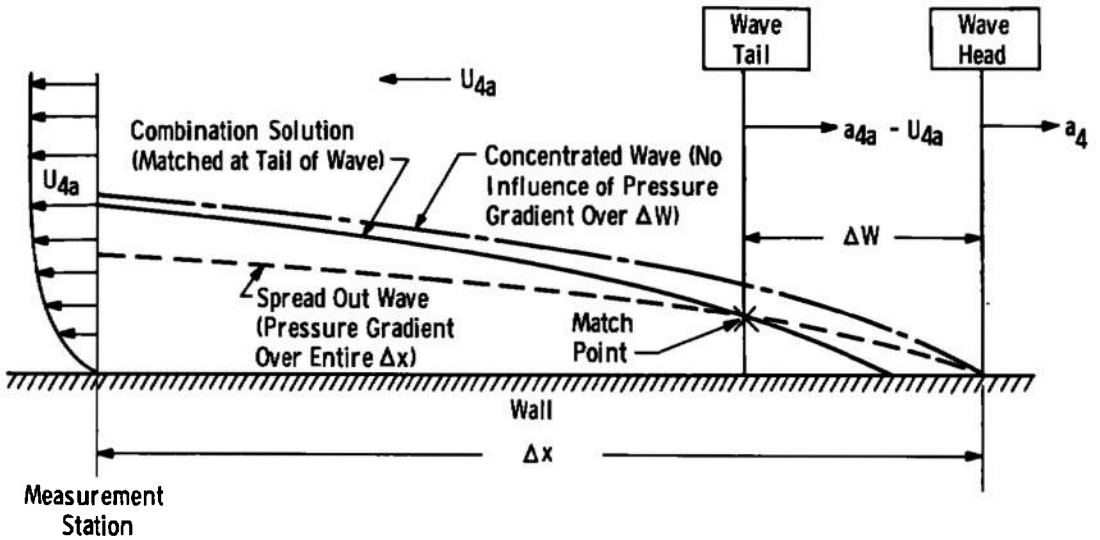

Fig. 24 Schematic Illustrating Charge Tube Boundary-Layer Edge for Various Theoretical Solutions

gradient in the wave, and a relatively thin boundary layer results for a given Δx. If the wave is relatively thin (ΔW small compared to Δx), then the boundary layer will grow virtually without favorable pressure gradient and will be somewhat thicker for a given Δx. Becker's theory provides for a "matched" solution for cases of interest between the two extremes of a concentrated and completely spreadout wave. In Pilot HIRT, the early time-point measurements are in a boundary layer

which has grown almost completely within the wave, and the late time-point measurements are still influenced by the favorable pressure gradient in the wave (have not completely approached the concentrated wave case).

Becker's theoretical edge is shown for some cases in Fig. 21; and it can be seen that the predicted thickness is somewhat less than the experimental value. The wall shear stress equation used in his solution is valid for Reynolds numbers of 10^7 only, and these measurements are all at 10^9 or greater. Becker's theory has been modified to properly account for the high Reynolds number skin-friction coefficient among other things, and the predicted edge using the improved theory is shown for some cases in Fig. 21. The experimental data, along with Becker's theory and the improved theory, are plotted in another form in Fig. 25. It can be seen that the improved theory agrees closely with all the experimental data and that the influence of growth within the wave is properly predicted. The trend in boundary-layer thickness with increasing Reynolds number is adequate but will be studied further.

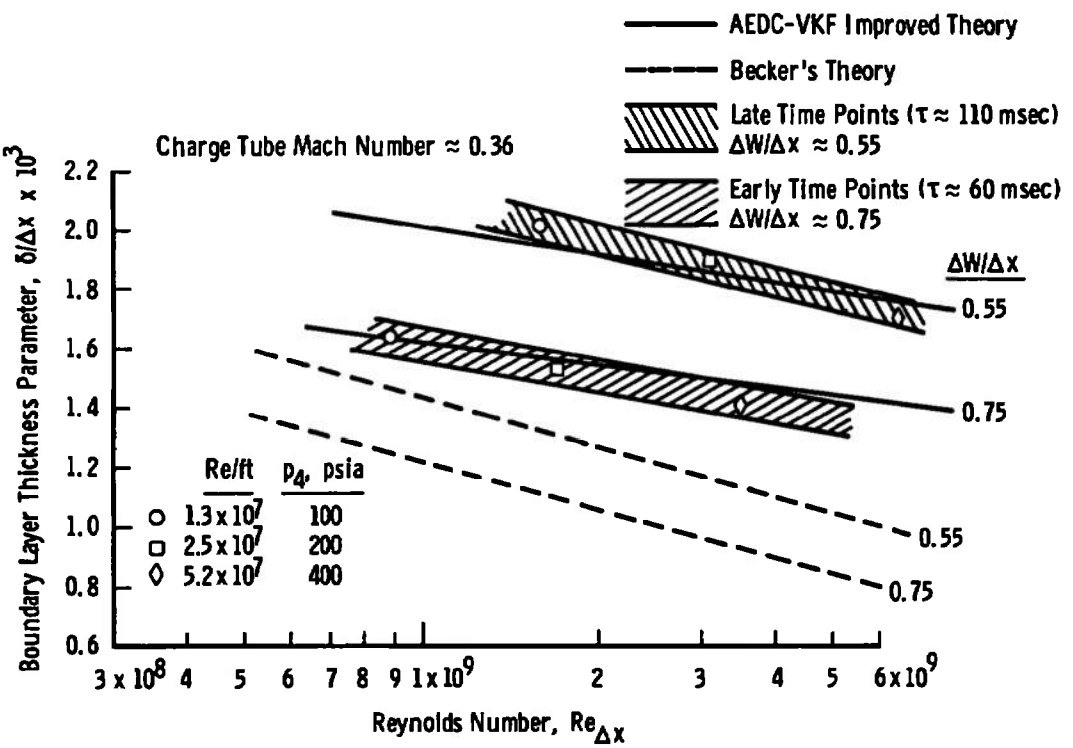

Fig. 25 Variation of Charge Tube Boundary-Layer Thickness Parameter with Reynolds Number for Early and Late Times

A typical boundary-layer profile obtained at the contraction exit is shown in Fig. 26. A theoretical calculation of the turbulent boundary-layer growth on a flat plate with both a starting profile similar to that observed at the charge tube exit and a favorable pressure gradient (as determined from the inviscid contraction) gives a good approximation to the experimentally observed profile. The profiles were found to be relatively insensitive to the amount of auxiliary flow through the porous wall. The auxiliary flow was varied from zero percent (porous walls sealed closed) to about 8 percent. It appears that this profile is primarily a result of the charge tube exit profile and the contraction ratio upstream of the measurement station, not the suction on the porous wall downstream of the measurement station. Similar profile data, taken at several times during the run, are plotted in Fig. 27. The variation in thickness with time is well behaved and similar to the boundary-layer growth at the charge tube exit. These profiles have been integrated to obtain the change in δ^* at the contraction exit, as shown in Fig. 27. A further group of boundary-layer profiles, taken in the test section at the center of model rotation, is given in Fig. 28. These are similar to the contraction exit profiles with the exception of their showing a slight effect on the profile near the wall due to the long run over the test section wall in zero pressure gradient.

If the change in δ^* with time at the contraction exit is considered, in the classical sense, to produce an area ratio (A/A^*) change, a Mach number variation of about 0.12 would be expected between 80 and 120 msec into the run on runs near Mach 1.0 based on the measured profiles. Experimentally, such a Mach number change has never been observed in the pilot tunnel even on repeat runs in the very sensitive range between Mach numbers 0.98 and 1.02. In this Mach number range, Mach number changes of less than 0.005 between 60 and 120 msec into the run are the norm. It is evident from this observation of the very constant test section Mach number with time, and the similiarity of boundary-layer growth with time at the three measurement stations, that no area ratio changes occur during a run. This should be true for all subsonic-transonically operated Ludwieg tubes where the choke point downstream of the test section can be expected to undergo boundary-layer growth similar to that in the charge tube.

The fundamental criteria, then, for the design of a high flow quality transonic tunnel using the Ludwieg tube storage system is that a uniform core exist in the test section for testing adequately sized models; however, the classic criteria which reflects the boundary-layer growth as an area change (and hence a flow property change) is only valid if the change in all areas with time is adequately considered (see Ref. 14 for an attempt).

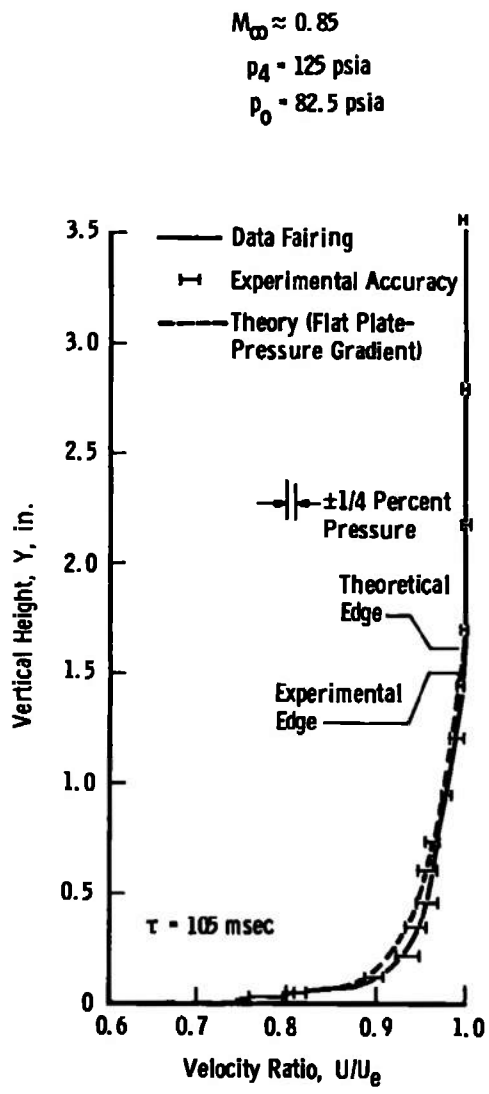

Fig. 26 Contraction Exit Boundary-Layer Velocity Profile

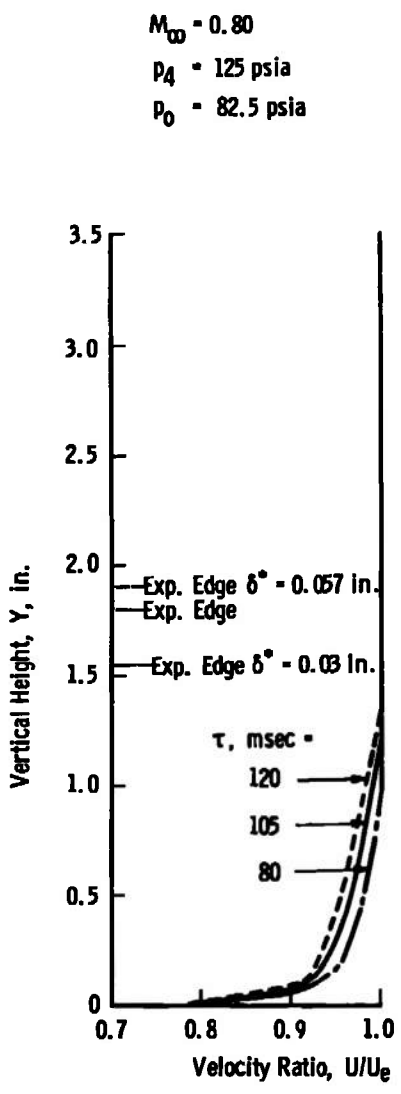

Fig. 27 Timewise Boundary-Layer Growth at the Contraction Exit

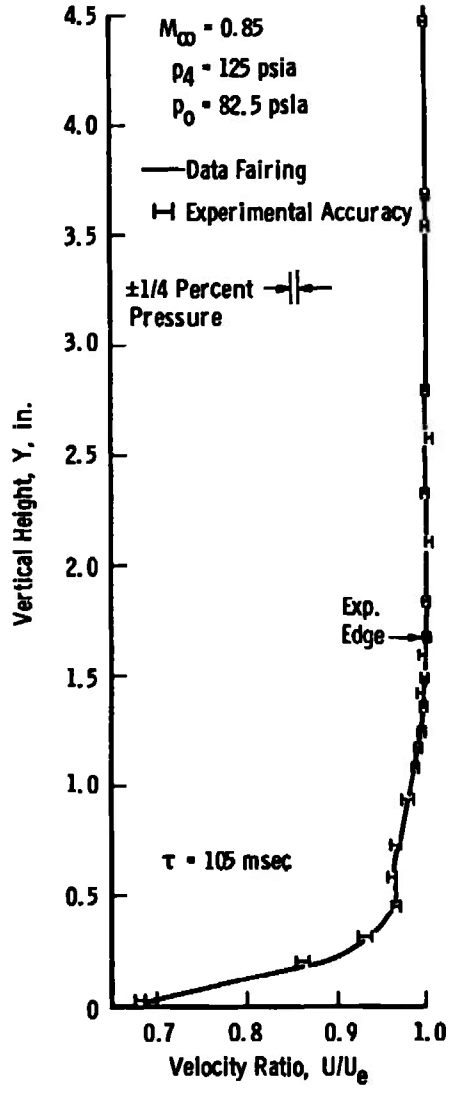

Fig. 28 Test Section—Center-of-Model Rotation Velocity Profile

2.4 AERODYNAMIC FLOW RESPONSE AT TRANSONIC SPEEDS

The fundamental question to be answered before advocating short-duration testing in any speed range concerns the time required for the flow field over the body to reach a steady-state condition. This will give the lower limit of test time required regardless of the frequency content of the test section aerodynamic noise or the response characteristics of force and pressure measurement instrumentation. The response of the inviscid flow field itself, the boundary layer, and separated flow fields (shock-induced or otherwise) must each be considered.

The flow response time is a function of the size of the body over which the flow must adjust and the flow velocity at which the adjustment can occur. This can be expressed by the Thompson number, T, which is

$$T = \frac{t_r U}{\ell}$$

In general, there will be a nondimensional flow response time associated with the response of each type of flow field (inviscid, boundary layer, or separated flow), and it is important to determine their magnitudes.

An experiment was designed for the Pilot HIRT to obtain some concrete data on the response of the inviscid and boundary-layer flow fields about a body to a rapidly imposed change in body attitude at transonic speeds. The experimental apparatus is shown in Fig. 29. The 15-deg semiangle cone model with a base diameter of 1.75 in. was positioned initially at an angle of attack of -4 deg and then displaced to +4 deg angle of attack. After the tunnel starting process was completed and the test section flow conditions stabilized, the system was actuated to impose a rapid cone attitude change. The model required 4 to 6 msec to traverse the 8-deg sweep. The exact instants at which the model began motion at -4 deg and ended motion at +4 deg were determined from a simple electrical contact system. There was no measurable change in plenum pressure induced by the model motion either above or on the side of the test section. A fast-response differential pressure transducer with less than 1/4-msec response to a step input was mounted inside the model with surface pressure orifices on the most windward and leeward rays at the same x/ℓ. The length from the nose of the cone to the pressure orifices was 2.9 in.

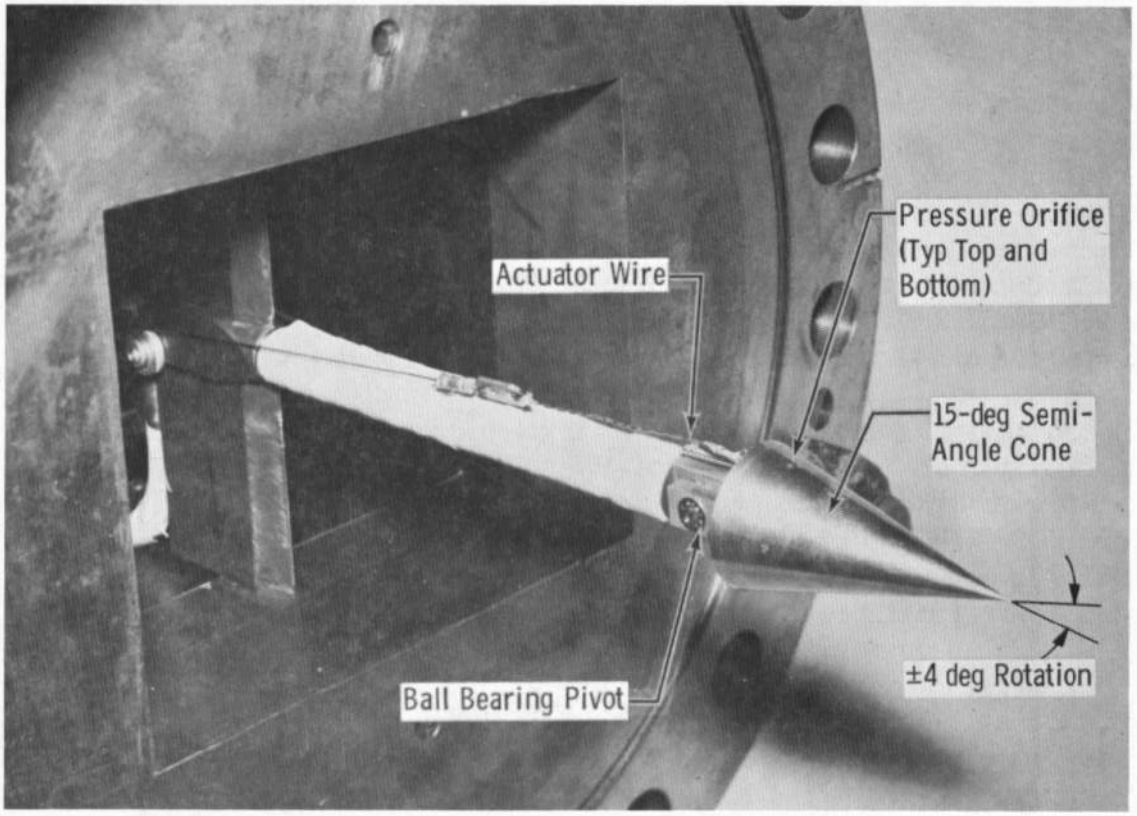

Fig. 29 Photograph of Flow Response Model Installation

It was found that the time required for the differential pressure to stabilize at the value dictated by the +4-deg angle of attack was less than 1/2 msec from the instant the model arrived at that position. The nondimensional response time which can be derived from these data on an inviscid and boundary-layer-dominated flow field is

$$T \lesssim 1.7$$

The response of the boundary layer itself to time-varying inviscid flow-field conditions has been studied experimentally and analytically in Refs. 16, 17, and 18. Wedge and flat-plate flows for both laminar and turbulent boundary layers at subsonic and supersonic conditions have been evaluated. These data show that for laminar boundary layers

$$T \approx 2 \text{ to } 4$$

and for turbulent boundary layers

$$T \approx 1 \text{ to } 2$$

Testing in HIRT will generally be conducted at Reynolds numbers sufficiently large to insure turbulent boundary layers over the majority of the model, which makes the latter value of T the most reasonable for estimating purposes. Note that this value is in good agreement with the Pilot HIRT experimental results just presented which were obtained under a condition with turbulent boundary-layer on the model.

A very sophisticated and informative experimental study was conducted with an oscillating airfoil (Ref. 19) from which some estimates of the aerodynamic response of shock-boundary layer coupled and separated flow fields can be made. A two-dimensional NACA 6-series airfoil model with a chord length of about 7 in. was fitted with a movable control surface of 25-percent chord. The control surface was oscillated at various frequencies while the pressure distribution over the upper and lower airfoil surface and shadowgraph pictures of the shock location were obtained. The shock location moved over the upper airfoil surface as the angular position of the control surface changed. Also, the trailing edge flow became separated at the negative control surface positions. The slow response of the pressure tubing system and instrumentation invalidates this measurement for anything but time-averaged results. However, the shadowgraph pictures, which do not suffer from such limitations, give an accurate measurement of shock location versus time.

If the flow response length is defined as the length from shock location to the control surface trailing edge and the experimental resolution of shock location is estimated to be within 0.2 deg equivalent control surface angle, an approximate T can be established from these limited experiments. This value of nondimensional response time which can be associated with shock-boundary layer coupled and separated flow fields is

$$T \lessapprox 5$$

With the values of T established for these various types of flow, one can estimate flow response times for body sizes which are typical of the full-scale HIRT (8- x 10-ft test section). These calculations are presented in Fig. 30 for a typical transonic Mach number of 0.85. The flow response time is less than 40 msec for bodies as long as 6 ft.

This response time is very short when compared with the HIRT facility running time, and a combination pitch-pause and continuous sector sweep will be employed to fully utilize the test time.

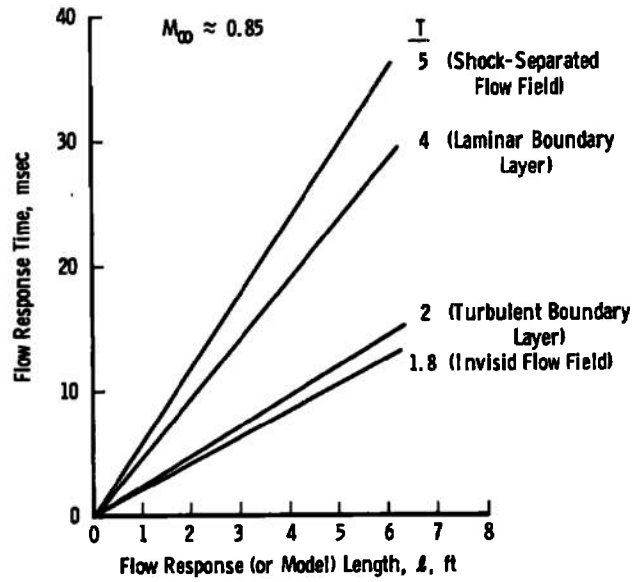

Fig. 30 Flow Response Time for Selected Flow-Field Types and Range of Body Lengths

2.5 PRESSURE DISTRIBUTIONS AND AERODYNAMIC FORCES ON SELECTED MODELS

Pressure and force measurements have been made on selected models in Pilot HIRT to demonstrate the feasibility of making such measurements in a short-duration transonic facility. In the process, of course, data were obtained which aid in analyzing transonic wall interference and Reynolds number effects.

A two-dimensional model of the C-141 wing (section normal to the wing leading edge at 38.9 percent of the semispan) has been tested in Pilot HIRT. This model is similar to the configuration which has been under extensive study by others (Refs. 20 and 21). Tests have been conducted at free-stream Mach numbers of 0.75 to 0.85, angles of attack of 0 and 2 deg, and at-chord Reynolds numbers of 2.7×10^6 to 15×10^6. The airfoil, shown in Fig. 31, has a chord length of 2 in. The pressure distribution is measured at 15 locations on the upper airfoil surface only. The pressure tubes are 0.045 I.D. with six 0.02-diam feeder holes each, as shown in Fig. 31.

The model has a 3.2-percent blockage in the test section which is comparatively large but could not be decreased since the model is already of minimum practical size. The airfoil size was chosen from the interplay of tube response (diameter) requirements, desired number of pressure measurements, tunnel blockage, and allowable model stress levels. To help alleviate some of the blockage effects, the airfoil was mounted perpendicular to the longer side of the test section rectangle, 1/2 in. off centerline, with the lower surface closer to the tunnel wall. A view of the model installation in Pilot HIRT is given in Fig. 32.

The pressure distributions measured on the upper surface of the airfoil at Mach 0.80 and model angle of attack of zero are plotted in Fig. 33. At this condition, an extensive supercritical flow region existed on the upper surface. These pilot tunnel results are in good agreement with the low blockage (≈0.04 percent) measurements made on a 6-in. chord airfoil in AEDC 16T and exhibit the same trends with wall porosity variation as the 0.7-percent blockage data on the same model in AEDC 4T (Ref. 21). The slight disagreement in pressure distribution at about the 15-percent chord location probably results from small model dimensional differences that were detected. The HIRT airfoil was 1 to 5 thousandths of an inch thicker than prescribed which corresponds to up to 2 percent in local thickness. The pressure distribution for a range of chord Reynolds numbers is shown in Fig. 34. Some shock movement in the rearward direction and an increasing trailing-edge pressure coefficient is evident as the Reynolds number increases. The magnitude and direction of these changes are similar to the results given in Ref. 20.

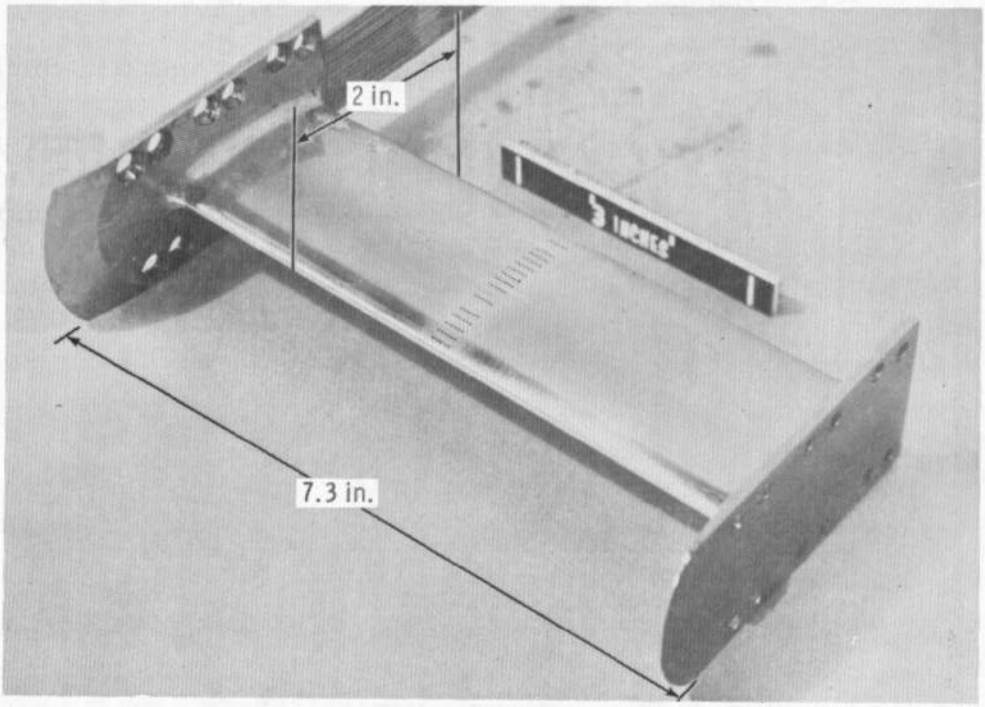

Fig. 31 Photograph of the Two-Dimensional, C-141 Airfoil Model

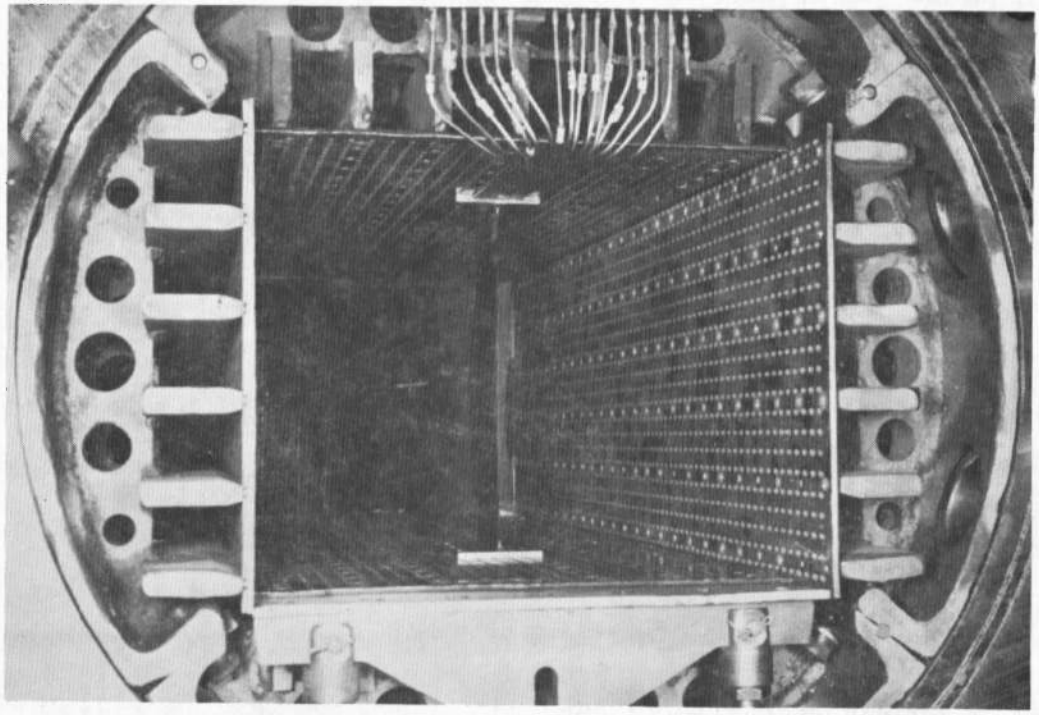

Fig. 32 Installation of the C-141 Airfoil Model in Pilot HIRT

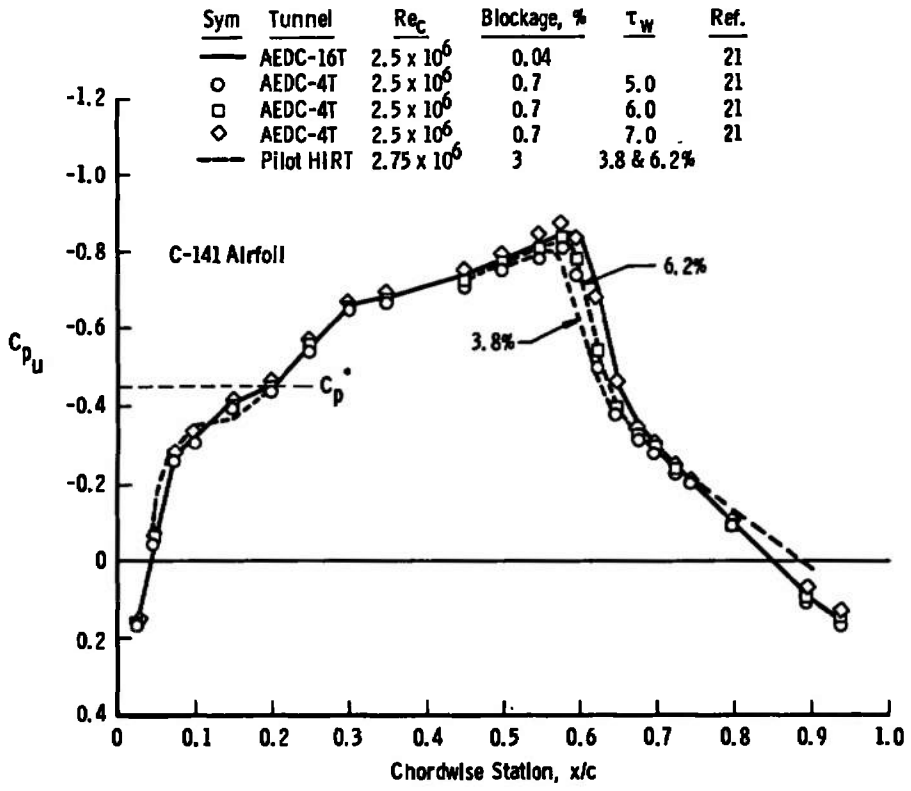

Fig. 33 Tunnel Wall Porosity Effects on Pressure Coefficient Distribution, $M_\infty = 0.80$, $\alpha = 0$, Upper Surface

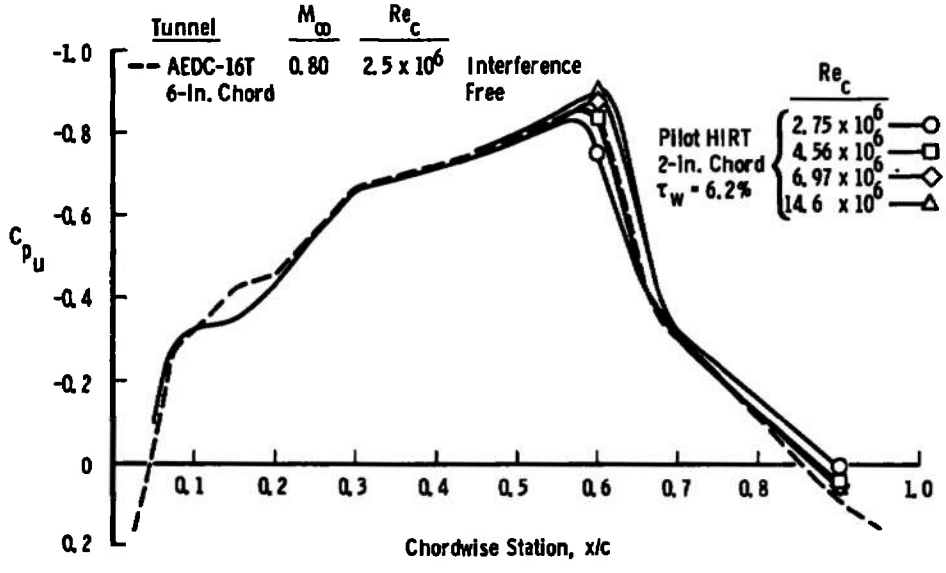

Fig. 34 Pressure Coefficient Distribution on the Upper Surface of the C-141 Airfoil for a Range of Chord Reynolds Numbers, $M_\infty = 0.85$, $\alpha = 0$

The pressure distributions measured at Mach 0.85 and zero angle of attack are plotted in Fig. 35. In this case, both a supercritical flow region and an extensive trailing-edge separation existed on the upper surface. These results are also in good agreement with those of Refs. 20 and 21.

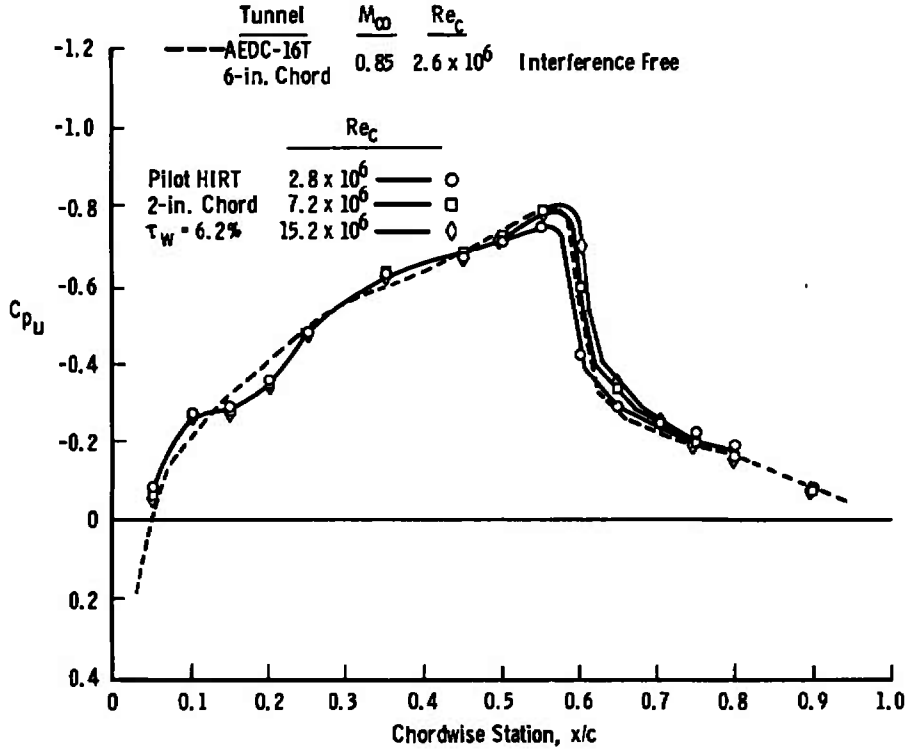

Fig. 35 Pressure Coefficient Distribution on the Upper Surface of the C-141 Airfoil for a Range of Chord Reynolds Numbers, $M_\infty = 0.85$, $\alpha = 0$

These data and the other high Reynolds number results do not exhibit the expected sensitivity to Reynolds number changes. The shock location on the 2-D airfoil does not move appreciably when compared to the shock movement on the full-scale C-141 configuration. Cahill concludes that the rear separation on the airfoil, and, hence, the shock location, could be strongly influenced by the proximity of the engine nacelles and trailing-edge construction break to the $\eta = 0.389$ station (Ref. 20). Neither of these characteristics was simulated in Cahill's swept panel test or the AEDC two-dimensional tests. Once separation occurs (regardless of the specific forcing function), the aerodynamics become highly sensitive to the Reynolds number; hence, differences between wind tunnel and flight data are present.

A series of force measurements has been made on 12-1/2- and 15-deg semiangle cones in Pilot HIRT. It was the intent of these measurements to insure that the timewise nature of the aerodynamic force produced by the flow was as expected from the pressure measurements discussed previously and that no unexpected measurement problems existed. The tunnel solid blockage of the models was varied from 0.7 to 3.6 percent, and the sting-to-model base diameter ratio ranged from 0.2 to 0.6. The Reynolds number based on model base diameter varied from 1.7×10^6 to 4.1×10^6.

A three-component, load-cell-type balance was used during the experiments. The strut which supported the sting-model was simply attached to the diffuser wall with no provision for isolation from the tunnel vibration. It was found that filtering was entirely adequate to minimize the variation in force produced by the tunnel vibration during the run. A sample trace of the axial and normal-force variation during the run is given in Fig. 36. It can be seen that the forces become constant (within the mechanically induced variation) at the same time that the tunnel stabilizes on Mach number. The force also remains constant until the return of the reflected expansion wave.

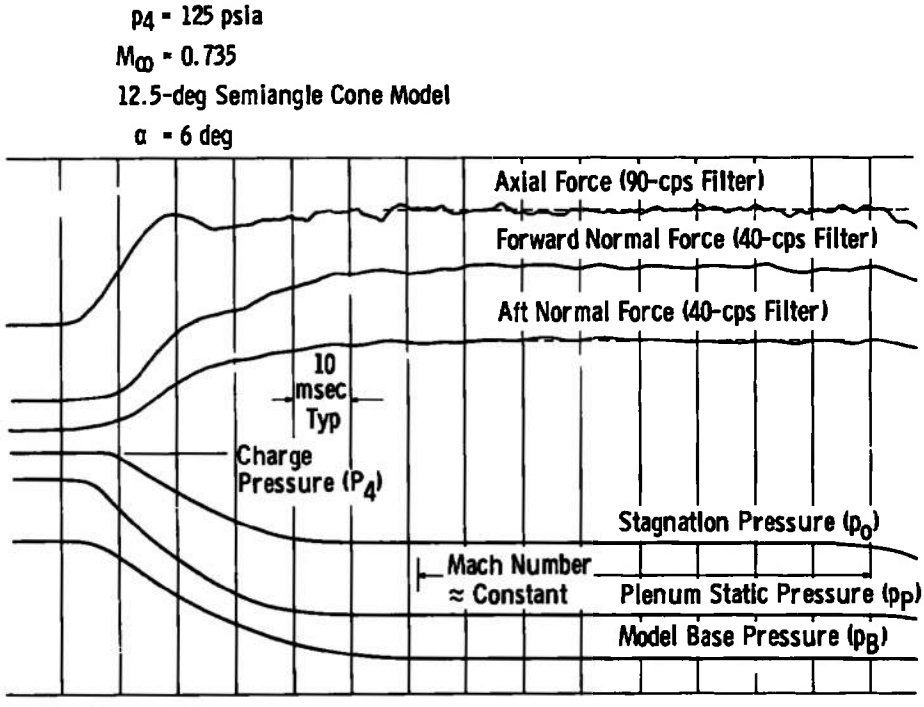

Fig. 36 Model Force and Pressure Variation during Typical HIRT Run

The model forces which were measured in the transonic regime are influenced by the physical blockage of the model in the tunnel and the size of the sting in relation to the body. Streamlines are restrained from adjusting about the body properly either by the presence of a wall with insufficient or improper cross-flow characteristics or by the presence of sting which is too large at the model base. Both of these effects can produce comparable errors in the base drag and the forebody drag. A range in both of these parameters was investigated in Pilot HIRT; however, only the lower blockage and smaller sting-to-base diameter ratio, ds/D, results will be discussed.

The total drag rise on a 12-1/2-deg semiangle cone is plotted in Fig. 37 for two blockages where the tunnel was operated at a fixed porosity of 6 percent. The data are compared to the results of Ref. 22, and it can be seen that the HIRT results approach these data as the blockage decreases. This is exactly as expected based on the blockage study described in Refs. 23 and 24 for a fixed-porosity transonic tunnel. In conjunction with the Pilot HIRT test, a series of experiments was conducted in the NASA-MSFC 14-in. transonic tunnel (Ref. 25) which has a variable-porosity, 60-deg inclined hole wall. The porosity schedule for the walls was opened 6-percent for Mach numbers up to 0.95, closed to about 1 percent at Mach 1.0, and then reopened to 3 to 6 percent at Mach 1.1 and 1.2, respectively. This schedule was developed from extensive wave reflection tests similar to those described in Refs. 2 and 26. Typical results from these tests are also shown in Fig. 37. Even at relatively high blockages, it can be seen that the drag rise in the variable-porosity tunnel is almost exactly the same as the low blockage data in the fixed-porosity tunnel.

The rise in forebody drag coefficient is plotted in Fig. 38 and again the HIRT data are in good agreement with previous results. Taken together, Figs. 37 and 38 indicate that the base drag is most strongly influenced by the blockage or ds/D at near Mach 1 since the total drag is the sum of the forebody and base drags. However, blockages of 2 to 3 percent have also been shown to produce significant variations in the forebody drag rise, as well as the base drag variation in a fixed-porosity tunnel, as evidenced by the data given in Ref. 27.

Sym	Source	Blockage, percent	ds/D	Re_D	
○	Ames	0.55	0.33	1.4×10^6	Fixed Slotted Wall, Ref. 22
———	Pilot HIRT	0.7	0.35	1.7×10^6	Fixed Porosity Wall, 6%
– – –	Pilot HIRT	1.2	0.26	2.3×10^6	Fixed Porosity Wall, 6%
□	NASA-MSFC 14"x14"	1.6	0.31	1.4×10^6	Variable (1-6%) Porosity Wall

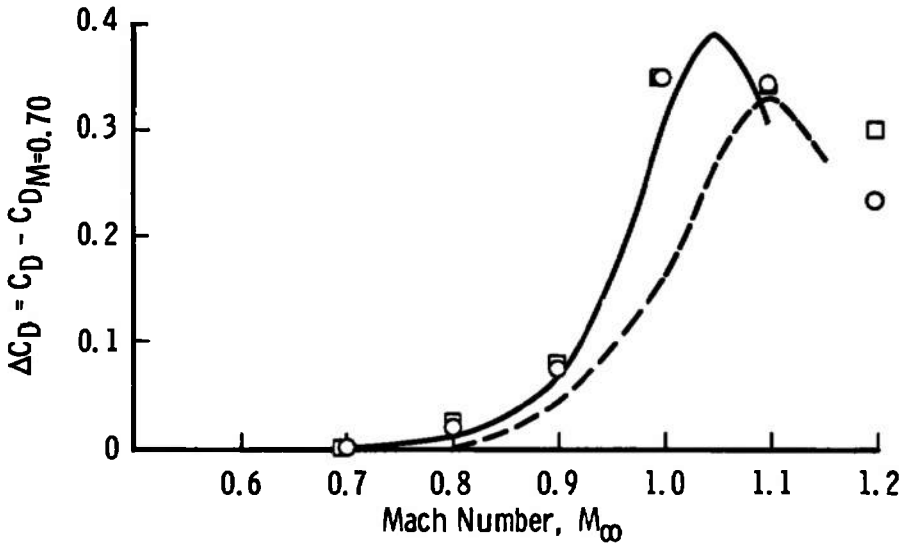

Fig. 37 Transonic Rise in Total Drag Coefficient, 12.5-deg Semiangle Cone

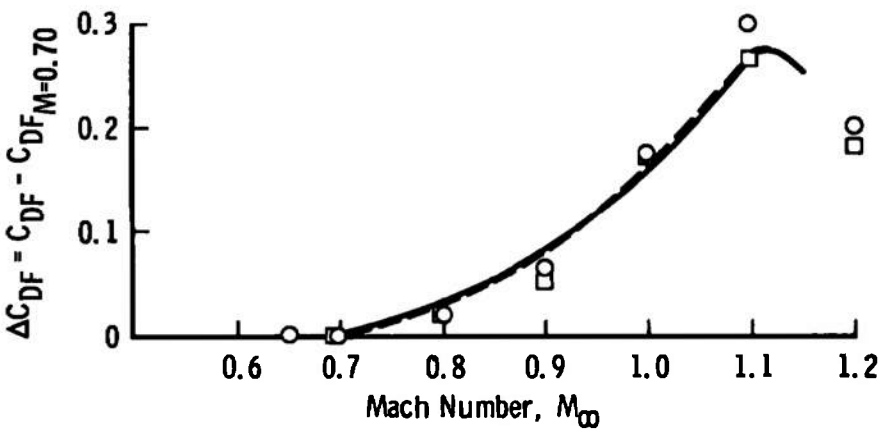

Fig. 38 Transonic Rise in Forebody Drag Coefficient, 12.5-deg Semiangle Cone

Similar results obtained on a 15-deg semiangle cone are plotted in Figs. 39 and 40 where the trend of the Pilot HIRT data is exactly as expected. The variable-porosity MSFC data can be considered to be analogous to 0.5-percent blockage fixed-porosity data (based on the 12-1/2-deg cone results given in Figs. 37 and 38). It certainly appears

that the transonic drag data taken in Pilot HIRT are in complete agreement with similar data taken in other long-duration transonic facilities within the constraints of tunnel blockage.

Sym	Source	Blockage, %	αs/D	ReD	
□	NASA-MSFC 14 x 14 in.	1.2	0.36	1.2×10^6	Variable (1 to 6%) Porosity
——	Pilot HIRT	1.2	0.26	2.3×10^6	Fixed Porosity Wall, 6%

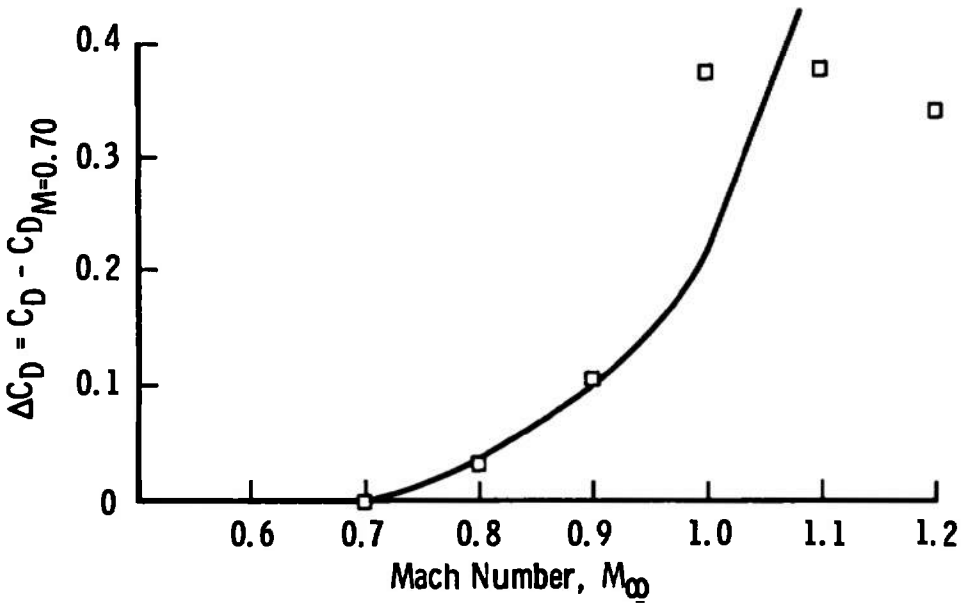

Fig. 39 Transonic Rise in Total Drag Coefficient on a 15-deg Semiangle Cone

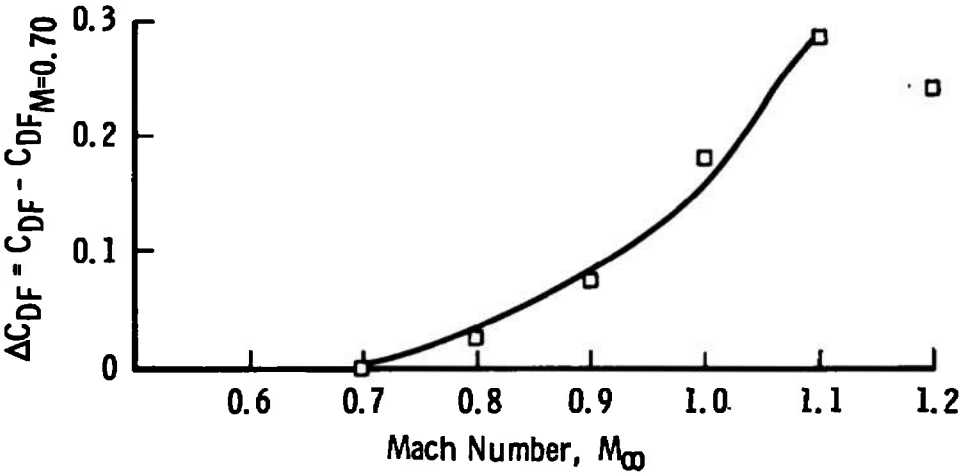

Fig. 40 Transonic Rise in Forebody Drag Coefficient on a 15-deg Semiangle Cone

Limited normal-force and pitching-moment data were also taken during the test and found to be in good agreement with the results of Refs. 22 and 27.

SECTION III
RELATED RESEARCH STUDIES

3.1 PLENUM VOLUME STUDY

As noted earlier, during the HIRT starting process, passage of the rarefaction waves through the test section causes the pressure in the plenum chamber to adjust as the test section pressure is reduced. During this process and before an equilibrium test section flow is established, a large fraction of the air in the plenum must be removed through the porous walls. Since the total flow time for the full-scale HIRT is about three seconds, it is essential to minimize the time to establish the test section flow. This may be accomplished by keeping the plenum volume as small as is practical. In addition to the start-time benefits, reduction in the plenum size results in considerable faciltiy cost savings.

The effect of plenum volume on transonic wind tunnel performance is relatively unknown, and in the beginning of the HIRT studies the authors knew of only two published investigations of the effects of plenum volume (Refs. 28 and 29). These were conducted with slotted-wall test sections. Presented in Ref. 29 are the results of an experimental investigation of the influence of plenum size (i.e., depth and slotted-wall length) on the zero-lift interference characteristics of a circular arc half model mounted on one wall. Variations of the depth and length of the plenum for the opposite wall and model blockage were found to have little influence on either the average plenum pressure or interference characteristics of the test section when the plenum volume to test section volume was greater than unity ($V_P/V_T > 1$).

Since little is known about the effects of plenum volume on perforated wall transonic wind tunnels, experiments were conducted in support of HIRT to study the effects of plenum volume on the test section flow characteristics (Ref. 30). Information acquired included free-stream Mach number distributions, wave-cancellation properties of perforated walls, force data on a delta wing model, and tunnel acoustic data which were used to evaluate the influence of plenum volume to test section volume ratios from 8.3 to 0.8. A volume ratio of approximately 9 represents the standard of most of today's transonic tunnels.

3.1.1 Apparatus

The tests were conducted in the AEDC-PWT 1- x 1-ft continuous-flow, nonreturn transonic wind tunnel equipped with a two-dimensional, flexible nozzle; perforated walls; and an auxiliary plenum evacuation system. The variable-porosity test section walls can be set for porosities from 0 to 10 percent; however, the installation of the auxiliary plenums to change the plenum volume made it difficult to change the wall porosity during the test. Therefore, the wall porosity was set at 3 percent for this investigation.

The effective plenum volume was varied by the use of three removable plenums that could be installed in the regular tunnel plenum. Plenum configurations and sizes hereafter referred to as standard (volume ratio 8.3), large (3.0), medium (1.8), and small (0.8) are shown in Fig. 41.

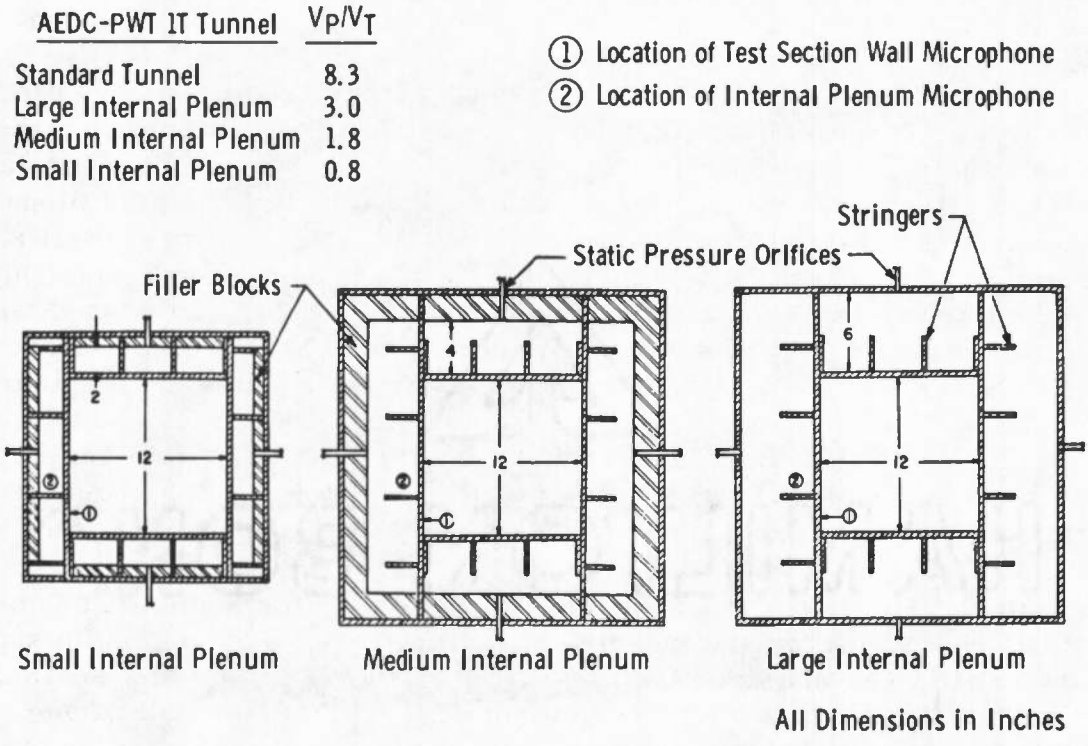

Fig. 41 Cross-Section View of Various Plenum Configurations

Local Mach number distributions along the centerline of the test section were obtained with a static pressure pipe having a total of 41 orifices spaced 2 in. apart. A 20-deg cone cylinder configuration used extensively at the AEDC and elsewhere for study of the effectiveness of porous walls in attenuating shock reflections was used in the current tests. Tunnel blockage of the model was 1 percent. AGARD Calibration Model B has been used extensively for comparison of force and moment data between facilities. At zero angle of attack, the tunnel blockage was 2.5 percent. The AGARD model used in the plenum volume studies is shown in Fig. 42.

3.1.2 Instrumentation

Model, static pipe, and tunnel pressures were measured with multitube mercury manometers and selected pressures were also measured with six precision transducers for on-line monitoring. Force data on the AGARD Model B were measured with a six-component internal strain gage balance, and base pressures were measured with a precision pressure transducer.

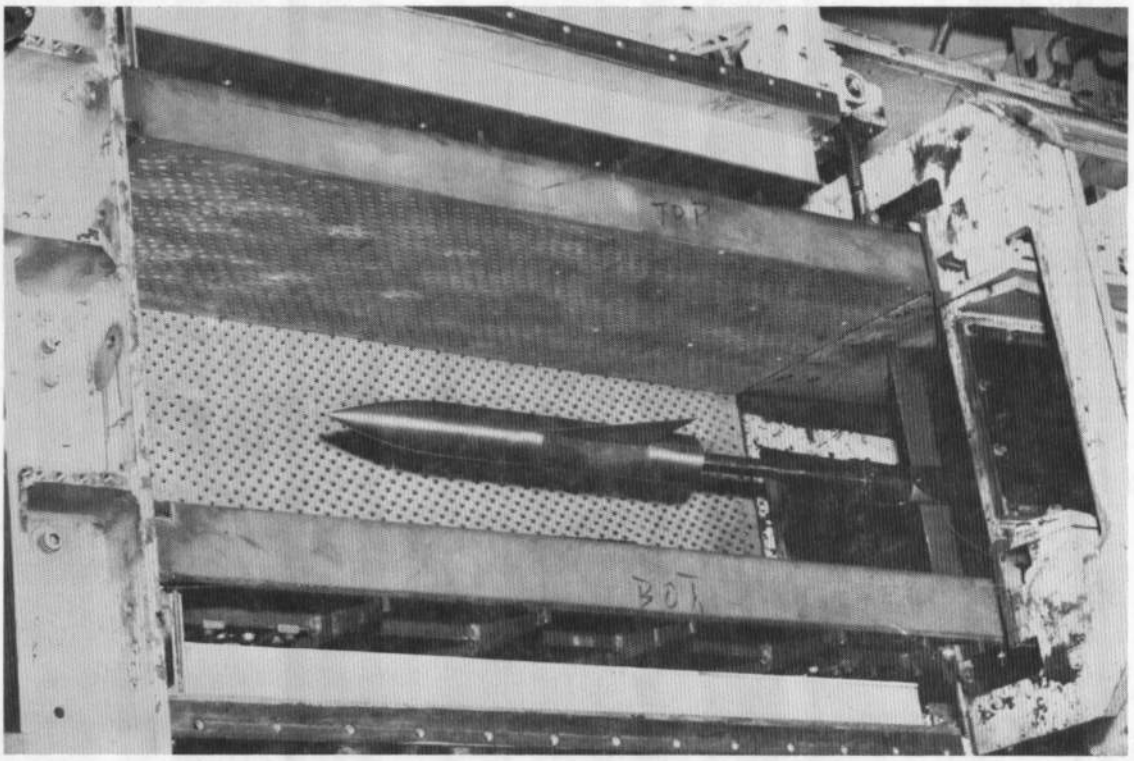

Fig. 42 AGARD Calibration Model B Installed in AEDC-PWT 1-ft Transonic Tunnel Test Section

Also considered in the investigation was the influence of the size of the plenum volume on the magnitude and frequencies of the fluctuating pressures in the test section. This possible influence was evaluated with microphones installed in the stilling chamber, in the test section wall immediately downstream from the nozzle exit in the internal plenums, and in the standard plenum. The test section microphone was installed with the diaphragm flush with the wall, and the plenum chamber microphones were installed in the forward region of each plenum in areas that were expected to have relatively low flow velocities. Vibration sensitivity of the microphones was evaluated with accelerometers integrally mounted with the stilling chamber and test section wall microphones. Locations of the test section and plenum microphones are shown in Fig. 41. The output of each microphone and accelerometer was measured using a root-mean-square (rms) voltmeter and recorded on magnetic tape for off-line spectrum analysis.

3.1.3 Procedure

The tests were conducted over the Mach-number range from 0.6 to 1.3 at stagnation pressures from 19 to 21 psia with the nozzle set at the sonic nozzle contour and the perforated walls set at 3-percent porosity. The experimental program consisted of three phases. During phase one, tunnel calibration data and centerline Mach number distributions were obtained for the three auxiliary plenum configurations using a centerline pipe. Static pressure distributions were obtained on a 20-deg cone cylinder in the second phase to investigate the effects of plenum volume variations on the ability of the perforated walls to eliminate compression and expansion wave reflections from the test section walls. In the third phase, the effects of plenum volume variations on force and moment data were investigated using AGARD Calibration Model B.

3.1.4 Centerline Mach Number Distributions

Representative test section centerline Mach number distributions obtained with the three plenum chambers are shown for M_∞ = 1 and 1.15 in Fig. 43. Also included for comparison is the Mach number distribution for the standard plenum configuration. The most notable influence of plenum size at Mach 1.15 occurred near station 20 for reasons yet unknown. An assessment of the Mach number distribution was made in terms of the 2σ Mach number deviations between stations 14.4 and 34.4 for all of the plenum configurations. Analysis of these

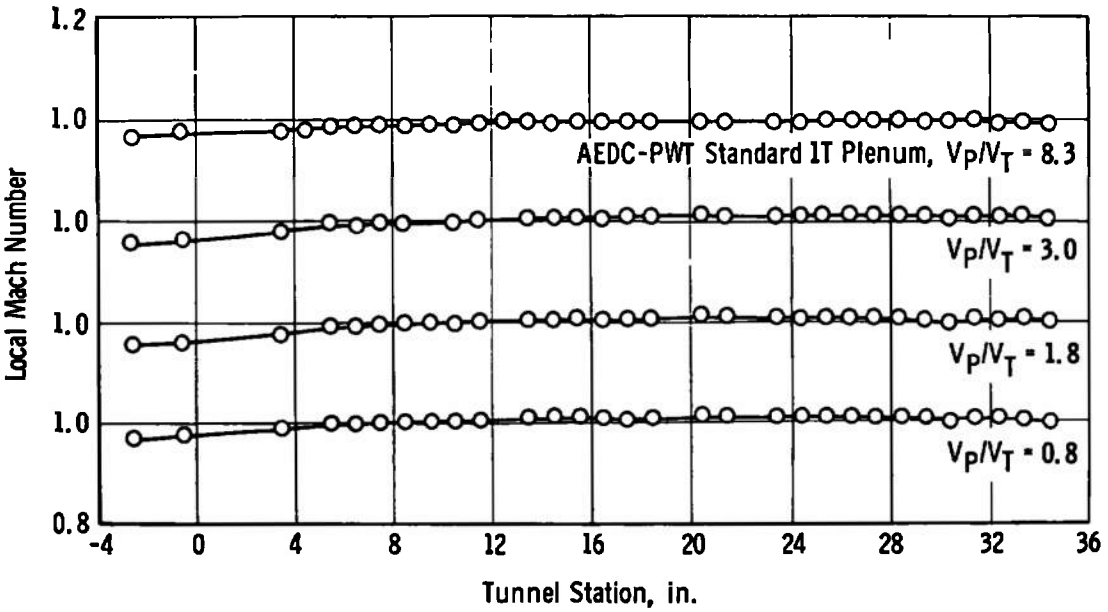

a. M_∞ = 1.0

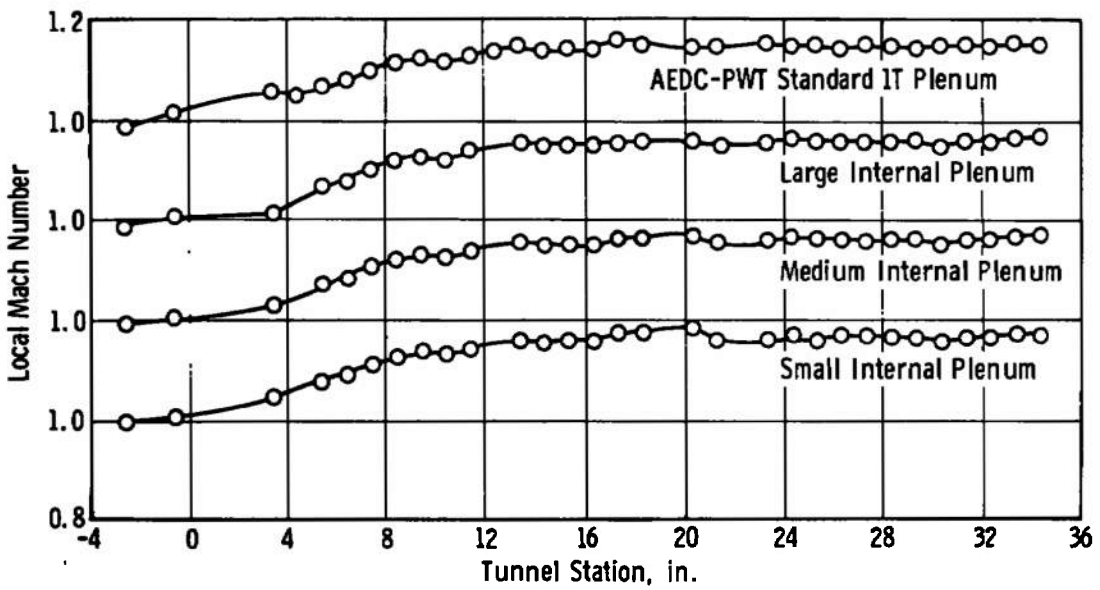

b. M_∞ = 1.15

Fig. 43 Effect of Plenum Volume in Centerline Mach Number Distribution

results shown in Fig. 44 indicates that below $M_\infty \approx 0.95$ variations in plenum volume had no measurable effect on the Mach number distribution. Above $M_\infty \approx 0.95$, decreasing the plenum volume increased the 2σ Mach number deviations when compared to the standard plenum; however, the 2σ Mach number deviations were approximately the same for the medium and large size plenums, $V_P/V_T = 1.8$ and 3.0, respectively. The departure of the 2σ Mach number deviations for the small plenum ($V_P/V_T = 0.8$) is primarily the result of the Mach number distribution near station 20 that was noted in Fig. 43.

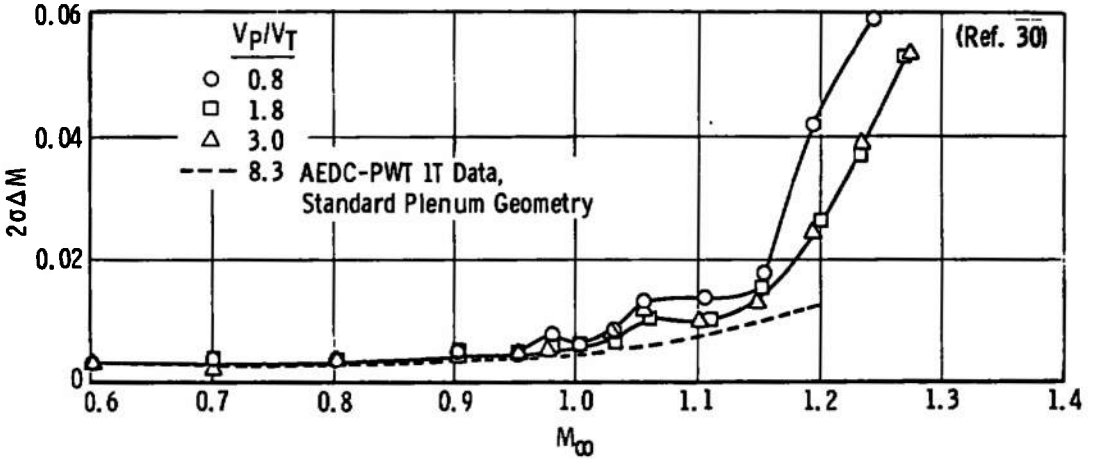

Fig. 44 Centerline Local Mach Number Deviation, Plenum Volume Effect

It should be noted that the internal plenums were open to the regular tunnel plenum only at the rear of the test section which required the removal of the entire mass flow from each wall to pass through the rear openings. This arrangement did not allow flow around the plenum from one area to another. Since most of the mass flow removal through the walls occurs ahead of station 14 at Mach numbers above 1, removal of the auxiliary plenum flow in the vicinity of the tapered porosity region would reduce the flow inside the plenum aft of station 14 and improve the Mach number distributions.

3.1.5 Cone-Cylinder Pressure Distributions

Pressure distributions on a 20-deg cone-cylinder model for three plenum configurations that are generally representative of results at all Mach numbers are compared with interference-free data from Refs.

31 and 32 at M_∞ = 1 and 1.15 in Fig. 45. At M_∞ = 1 and 1.15 there was little influence of plenum volume; however, the M_∞ = 1 results at x/D = 4 to 6 were not in agreement with the interference-free data. If the wall porosity were changed from the constant 3 percent, these effects would probably disappear. At Mach 1.15, the pressure distributions were in good agreement with the interference-free data.

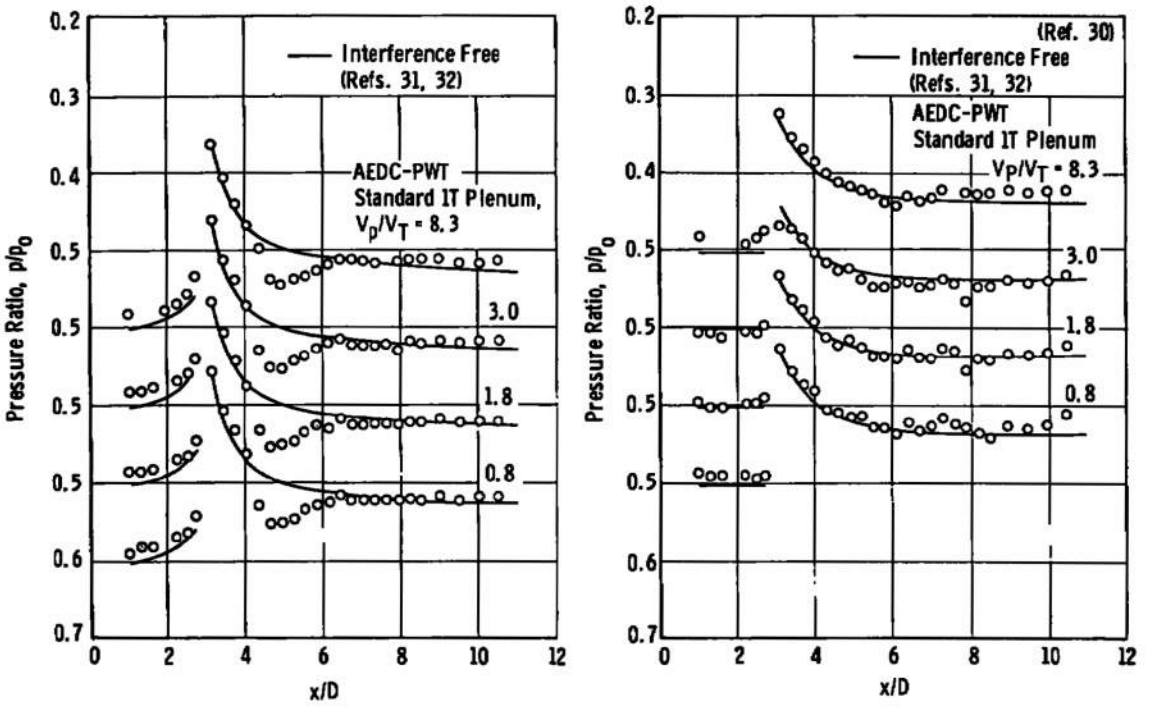

a. M_∞ = 1.0 b. M_∞ = 1.15

Fig. 45 Effect of Plenum Volume on Cone Cylinder Pressure Distribution

3.1.6 AGARD Model B Force Data

Decreasing the plenum volume had no significant influence on the lift and pitching-moment results; however, the forebody drag coefficient at Mach numbers above 1.05 increased with the small plenum, Fig. 46. No notable influence of plenum volume was found on the base drag.

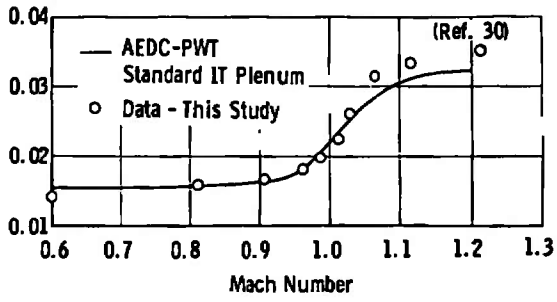

a. Small Plenum, V_P/V_T = 0.8

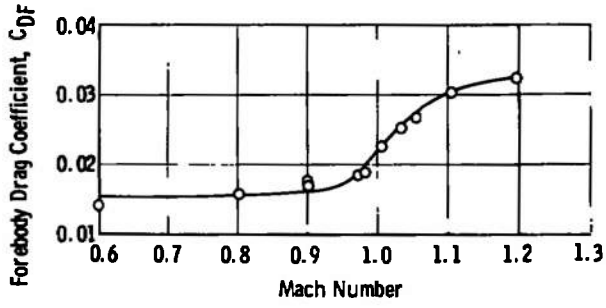

b. Medium Plenum, V_P/V_T = 1.8

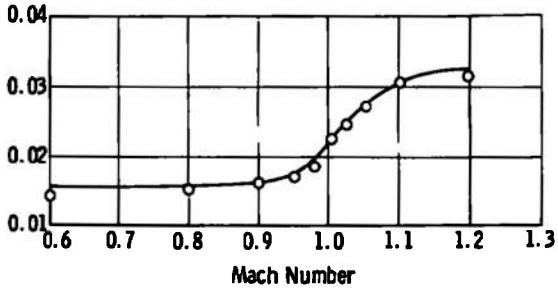

c. Large Plenum, V_P/V_T = 3.0

Fig. 46 Plenum Volume Influence on AGARD Model B Drag Coefficient

3.1.7 Acoustic Data

The test section wall acoustic data are presented in Fig. 47 to show only the relative influence of test section noise levels as a function of plenum volume size. The only significant effect of plenum volume was at Mach numbers below 0.9 where the small plenum and standard plenum basically produced the same test section sound levels, whereas the medium and large sizes had an effect at M = 0.6 and 0.8.

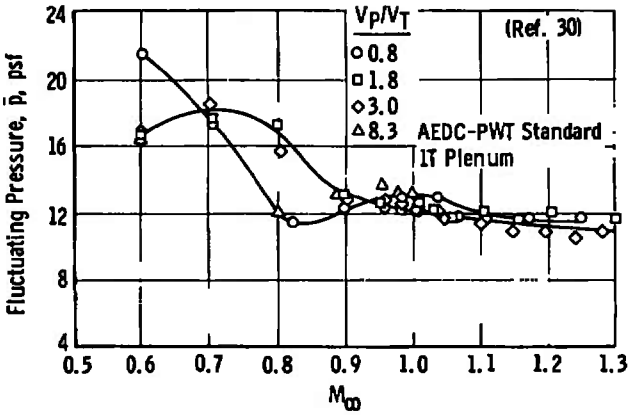

Fig. 47 Effect of Plenum Volume on Test Section Static Pressure Fluctuations

3.2 EXHAUST ACOUSTICS

The current national emphasis on environmental considerations of all types made the operational noise produced by the exhaust system of HIRT of prime interest in the early phases of conceptual design. The nature of the facility - i. e., blowdown to atmosphere, and the very high flow rates associated with the high Reynolds number operation of such a large tunnel produce a potentially hazardous noise environment equal to, if not beyond, the state-of-the-art in acoustic prediction technology. The facility is sited in an isolated area of AEDC (Fig. 48) to minimize the influence of the acoustics on existing facilities and inhabited areas. A comprehensive analytical and experimental investigation of the noise-generating mechanisms associated with the operation of the facility has been completed and reported (Ref. 33). Recognizing the limitations and possible errors of present prediction methods, this investigation relied heavily on a scale model test program which examined in detail the exhaust flow noise.

3.2.1 Description of Apparatus and Experiments

A one-thirteenth-scale model of the HIRT exhaust system was attached to a high-pressure storage system which allowed continuous operation over many seconds. Installation of the acoustic model is shown pictorially in Fig. 49. The dominant features of the model are the individual simulated start valves which are manifolded together inside of an exhaust stack as shown in the photograph in Fig. 50.

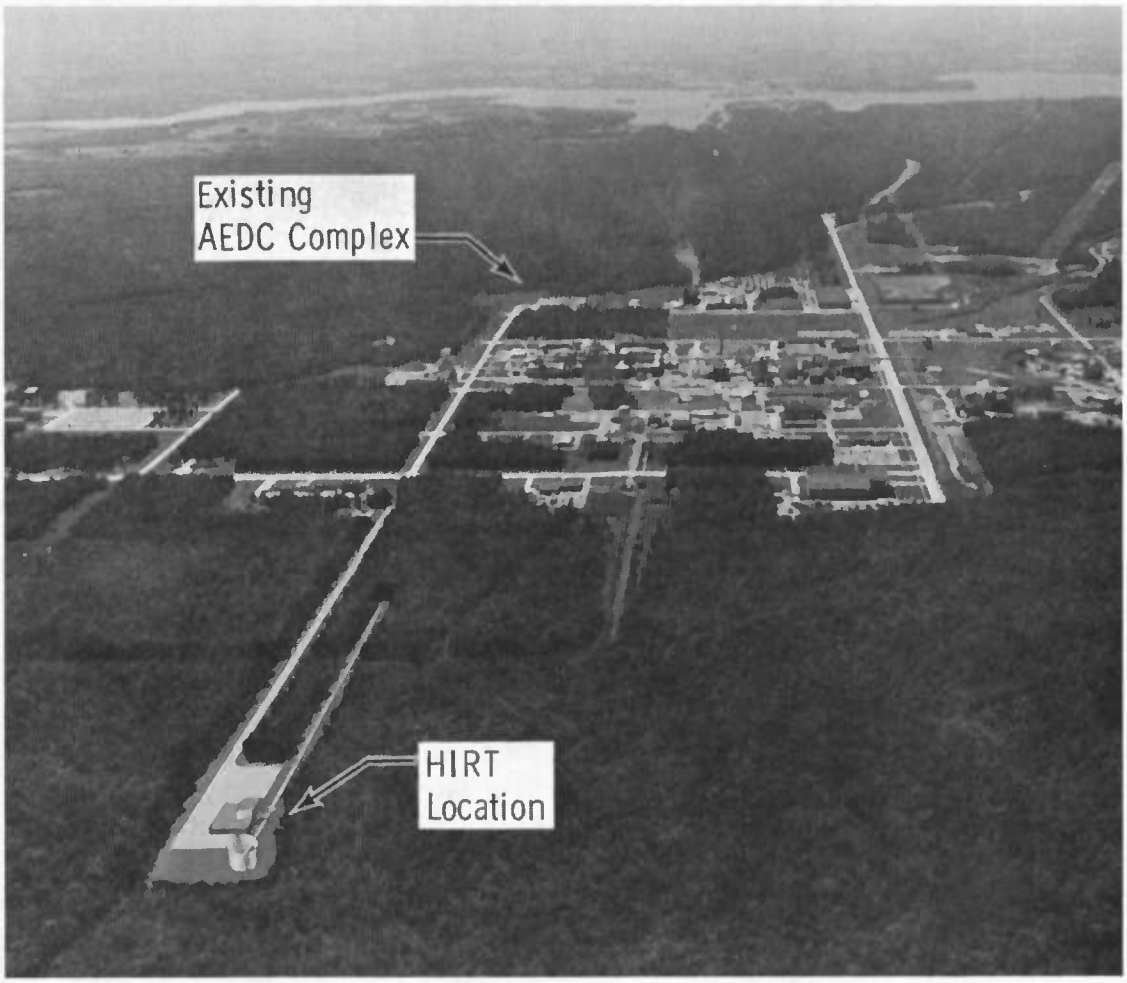

Fig. 48 Proposed HIRT Location in Relation to Existing AEDC Facilities

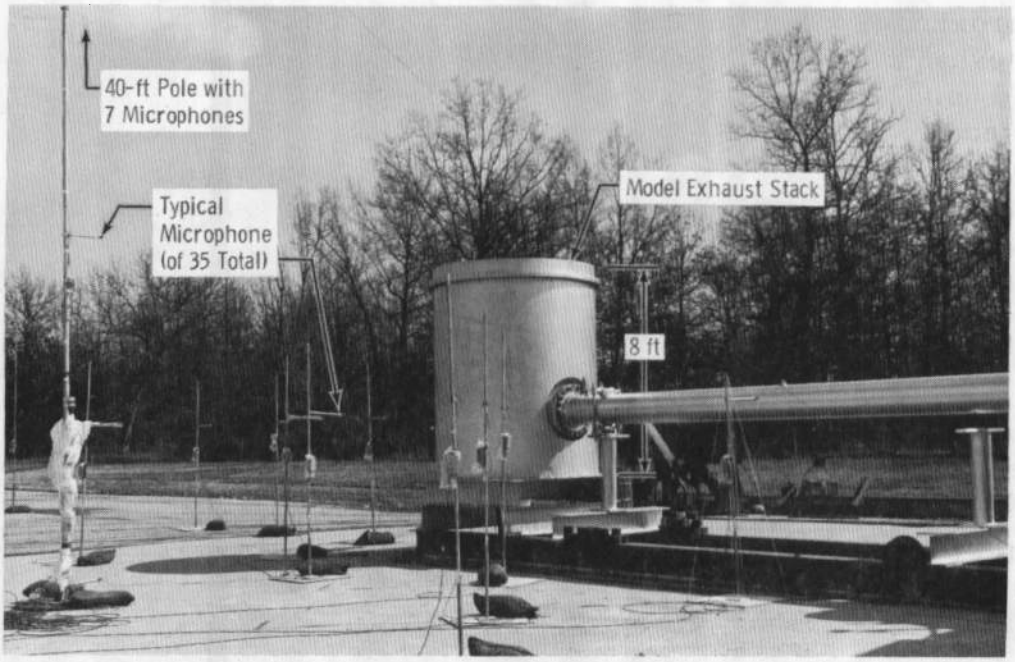

Fig. 49 Photograph of the 1/13-Scale Acoustic Model Facility of HIRT Exhaust System Showing Microphones and Stands

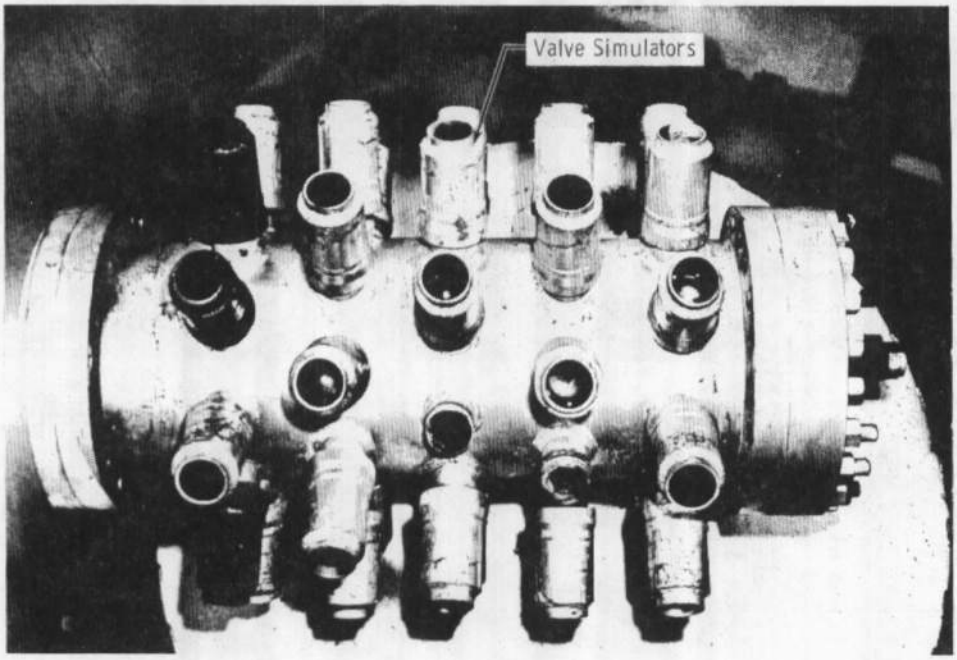

Fig. 50 Photograph of the 1/13-Scale HIRT Exhaust Manifold and Valve Simulators—View Looking Down into Exhaust Stack

Approximately 35 standard acoustic microphones were arrayed around the exhaust stack at distances simulating both the near-field and far-field noise dominated regions (Fig. 51). The model facility was operated at stagnation pressures of 250 to 500 psia and flow rates up to 650 lb/sec. Measurements of the spectral content and spatial distribution of the noise around the stack were made at each operating condition.

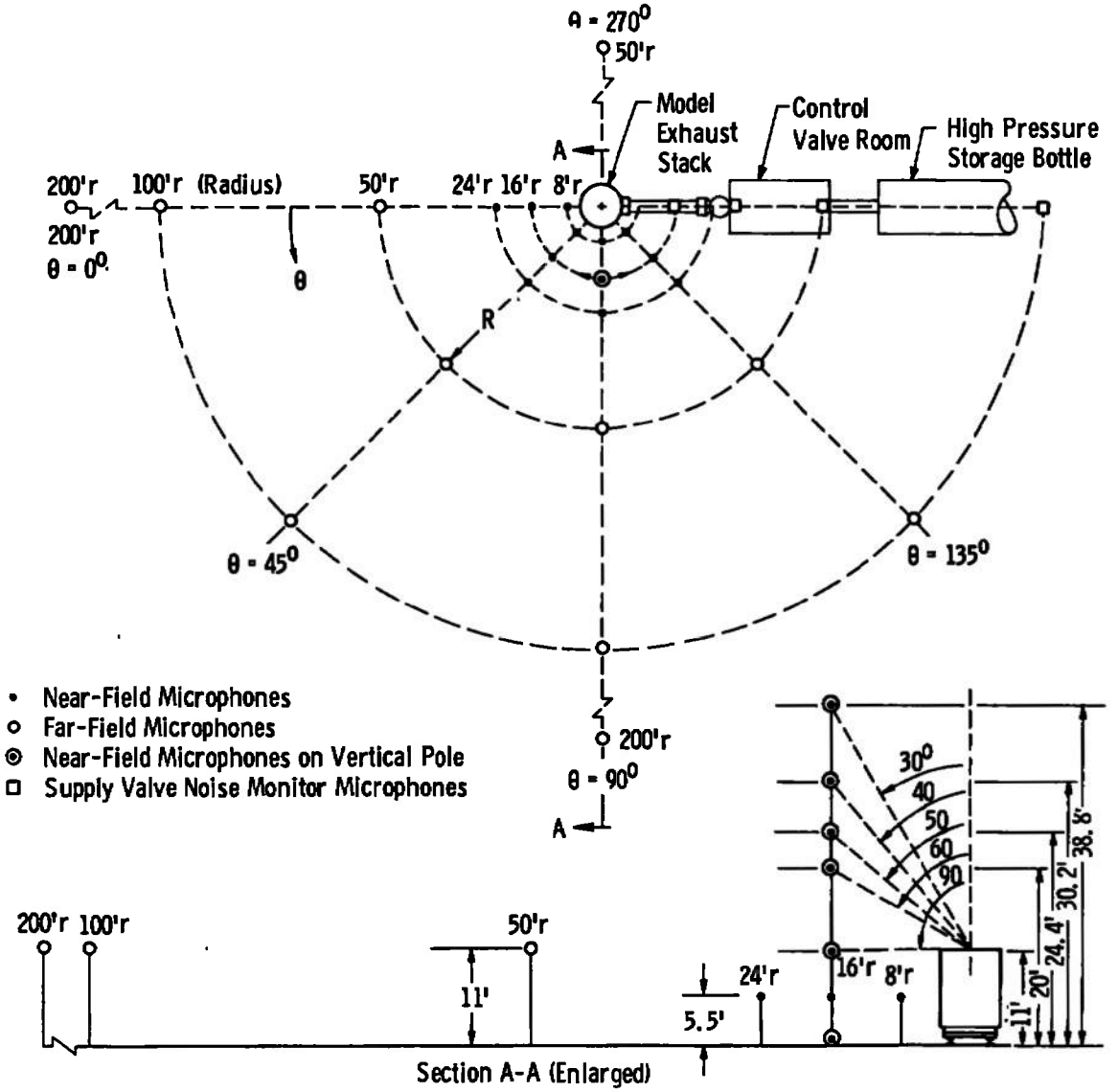

Fig. 51 Microphone Instrumentation Locations for Field Measurements of the Exhaust Flow Noise

3.2.2 Results and Application to Full Scale

To define the acoustic environment resulting from operation of the model facility, several characteristics of the noise field and the interrelationship of the noise with the facility operational variables are required. These include:

(a) Effects of total pressure and mass flow rate on the noise;

(b) Free-field directivity characteristics of the noise; and

(c) Spreading characteristics of the noise.

Both the starting noise (compression field produced by valves opening over 0.1 sec) and the steady state or running noise were evaluated. Because, in general, the starting noise was found to be less severe than the running noise (Ref. 33), only the steady-state results will be discussed. A typical experimental noise spectral distribution is shown in Fig. 52 for a range of radial distances from the exhaust stack center. Evaluation of these three noise field characteristics involved analyses of both the overall sound pressure levels and one-third octave band spectra of the experimental results. The following discussion is a synopsis of the detailed results presented in Ref. 33.

For various fixed values of mass flow rate, changes in stagnation pressure were found to have no influence on the overall sound pressure level. The implication of this result is that nature of the flow within the diffuser-manifold section has little influence on the noise radiated to the free field. Variations in the mass flow rate, on the other hand, were found to produce a very direct influence on the overall sound pressure level. A very repeatable increase in overall sound pressure level of 6db per doubling in mass flow was evident. Thus, for the purposes of predicting the full-scale noise from the model scale data, only the mass flow rate is required as a known operational parameter.

The directivity of the facility exhaust noise radiated to the free field was evaluated in a plane parallel to the ground and in a plane normal to the ground plane. No distinct directivity characteristics were evident in the plane parallel to the ground which indicates that the exhaust stack is effective in directing both the exhaust flow and the associated noise field in an upward direction. A pronounced directivity was evident in the plane normal to the ground plane with the peak noise measured at a height of 20 ft on the pole located as shown in Fig. 51. The data are clearly consistent with previous measurements of jet exhaust noise directivity and shielding. A distinctive shadow zone is

present at heights below the exit of the exhaust stack which has a large influence on the near-field acoustic sound pressure level. The data also show both destructive and constructive interference of the primary and ground reflected waves at specific radii from the exhaust stack as evidenced by the spectral shapes below 500 Hz shown in Fig. 52.

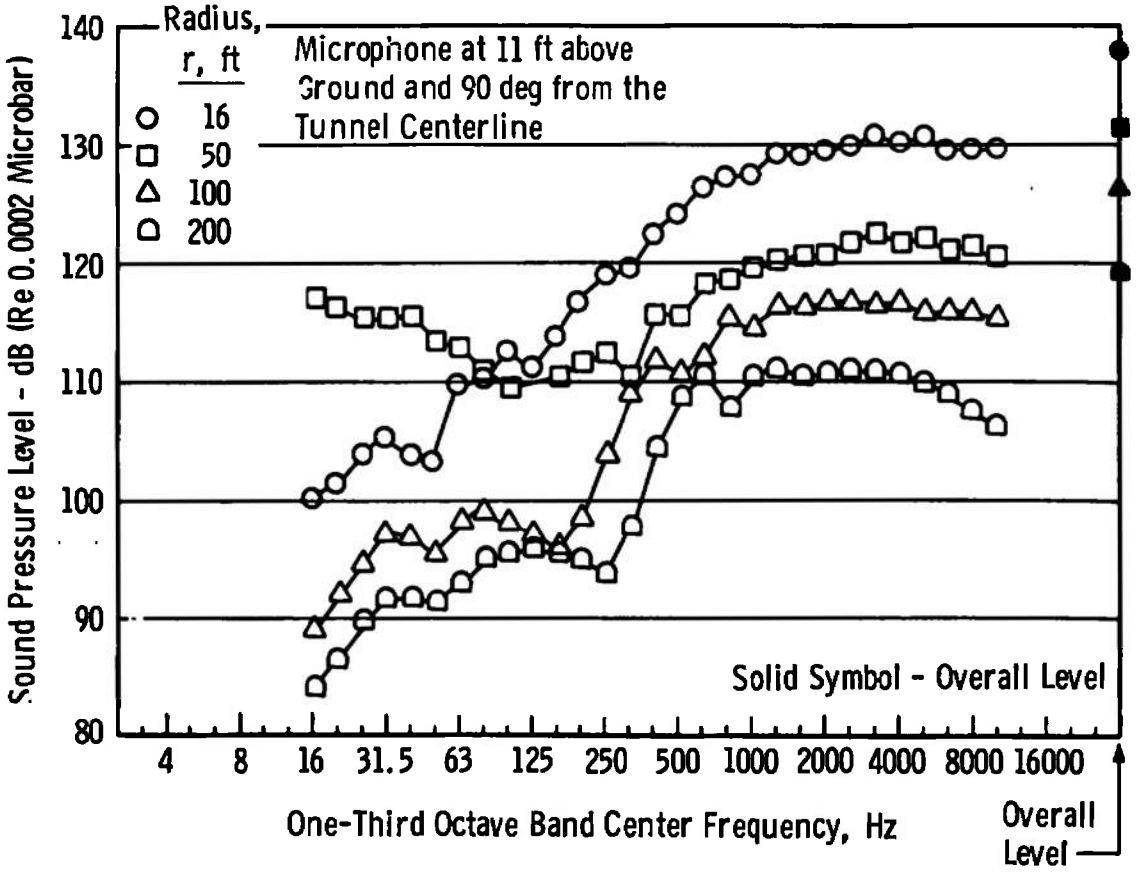

Fig. 52 One-Third Octave Band Spectra of the 1/13-Scale Model HIRT Exhaust Noise Showing the Effect of Radial Location on the Ground Plane Noise, p_o = 500 psia, W_T = 630 lb/sec

A composite plot showing the near-field directivity effects and the far-field spreading characteristics of the noise is given in Fig. 53. In the near field, the overall level is dominated by the distance above the ground level; and, in the far field, the noise level decreases at about 6 db per doubling in distance. The far-field model data are slightly affected by atmospheric absorption losses; however, the model data were corrected for these absorption effects prior to making full-scale HIRT estimates.

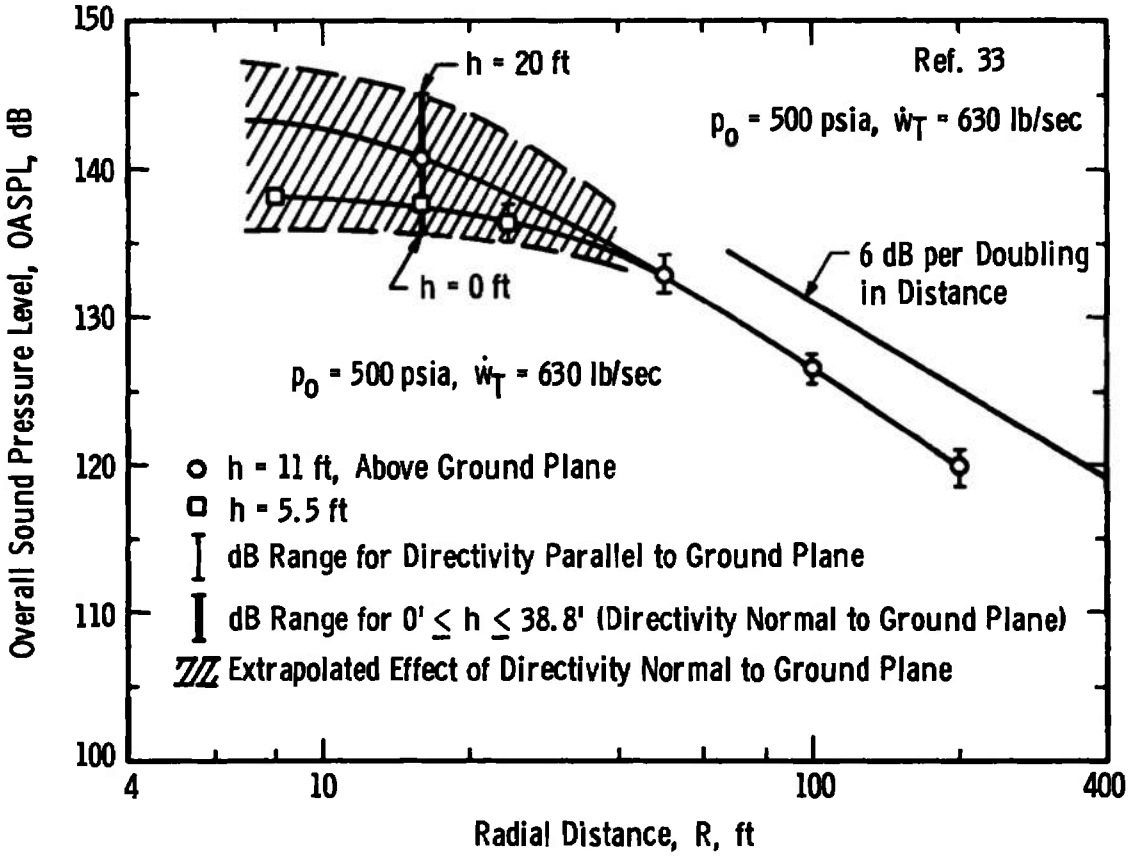

Fig. 53 Variations of Overall Sound Pressure Level with Distance and Height for the Maximum Model Test Condition

This detailed knowledge of the model spectral content, the scaling of spectral content with size, the directivity and spreading of the model exhaust noise field and the determination of the mass flow rate as a basic scaling parameter has resulted in the full-scale HIRT noise prediction given in Fig. 54. This represents the variation in overall sound pressure level with radial distance from the exhaust stack for the maximum full-scale operating condition (p_0 = 500 psi; M = 1.0). Included in this figure are estimates of the atmospheric absorption and attenuation from ground cover which have a significant effect on the far-field noise levels for the predicted frequency content of the full-scale exhaust noise. These overall sound pressure levels have also been weighted by appropriate subjective noise scales based on the predicted noise frequency spectrum to arrive at the "perceived noise" levels in controlled and uncontrolled areas surrounding the facility; see Fig. 55. The environmental impact of these exhaust noise levels is discussed in detail in Ref. 34.

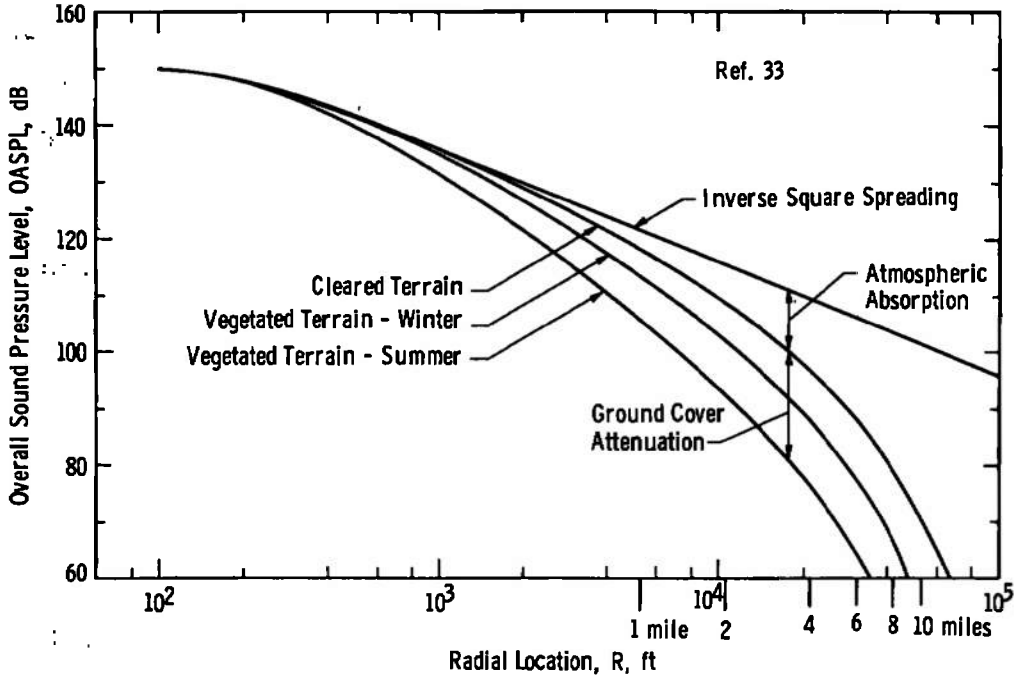

Fig. 54 Predicted Variation of OASPL with Radial Location for Full-Scale HIRT Facility Operating at Maximum Flow Rate ($\dot{W}_T$ = 160,000 lb/sec)

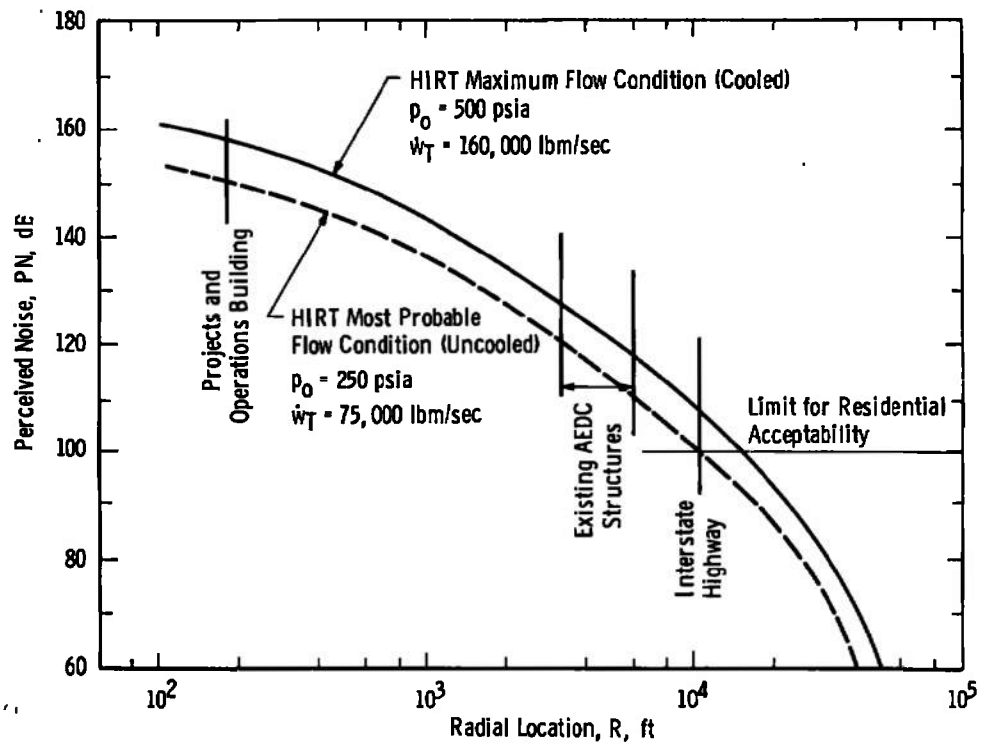

Fig. 55 Predicted Perceived Noise Intensities at Radial Distances from the Center of the Full-Scale Exhaust Stack for Two Operating Conditions and Assuming Winter Vegetation

SECTION IV
CONCLUDING REMARKS

In support of the development of the AEDC high Reynolds number transonic tunnel (HIRT), extensive use has been made of a 1/13-scale model of the facility. The studies included measurement and analysis of the boundary layers in the charge tube, entrance to the nozzle and in the test section, start time of the tunnel, flow quality in the test section, response time of the flow, pressure distributions on a two-dimensional airfoil model, force measurements on cones, an investigation of the influence of plenum volume, and an investigation of the acoustics of the exhaust system. The results of the experimental work demonstrate the feasibility of obtaining high Reynolds number aerodynamic data in a transonic tunnel with a Ludwieg tube drive system.

REFERENCES

1. "Facilities and Techniques for Aerodynamic Testing at Transonic Speeds and High Reynolds Number." AGARD-CP-83-71, August 1971.

2. Jacocks, J. L. "Determination of Optimum Operating Parameters for the AEDC-PWT 4-ft Transonic Tunnel with Variable Porosity Test Section Walls." AEDC-TR-69-164 (AD857045), August 1969.

3. Whitfield, Jack D., Schueler, C. J., and Starr, Rogers F. "High Reynolds Number Transonic Wind Tunnels - Blowdown or Ludwieg Tube?" Paper 29, AGARD-CP-83-71, August 1971.

4. Jacocks, J. L. and Hartley, M. S. "Calibration of the AEDC-PWT 4-ft Transonic Tunnel with Modified Walls." AEDC-TR-69-134 (AD853841), June 1969.

5. Boone, James R. and McCanless, George F., Jr. "Application of the Technique for Evaluating the Acoustic Sources of Background Noise in Wind Tunnel Facilities." Technical Report HSM-RO5-69, NASA CR 102623, Chrysler Corp., Huntsville, Alabama, March 1969.

6. Credle, O. P. "An Evaluation of the Fluctuating Airborne Environment in the AEDC-PWT 4-ft Transonic Tunnel." AEDC-TR-69-236 (AD861673), November 1969.

7. Credle, O. P. and Shadow, T. O. "Evaluation of the Overall Root-Mean-Square Fluctuating Pressure Levels in the AEDC-PWT 16-ft Transonic Tunnel." AEDC-TR-70-7 (AD864827), February 1970.

8. Mabey, D. G. "Flow Unsteadiness and Model Vibration in Wind Tunnels at Subsonic and Transonic Speeds." Aeronautical Research Council, London, England, CP No. 1155, ARC 32716, October 1970.

9. Robertson, Jack E. "Unsteady Pressure Phenomena for Basic Missile Shapes at Transonic Speeds." AIAA Preprint No. 64-3 presented at the Aerospace Sciences Meeting, New York, New York, January 20-22, 1964.

10. Becker, von E. "Das Anwachsen der Grenzschichtin und hinter einer Expansionwelle ("The Boundary Layer in and Behind an Expansion Wave)." Ingenieur-Archiv, Drittes Heft XXV Band, Vol. 25, No. 3, 1957, pp. 155-163.

11. Becker, von E. "Reibungswirkungen beim Rohr Windkanal." Paper No. 20, Aerodynamischen Versuchsanstalt, Gottingen, West Germany, 1958.

12. Hottner, Theo. "Untersuch ungen an einem Modell-Rohrwindkanal bei Machzahlen von M_a - 3 bis 6" ("Investigations with a Model Tube Wind Tunnel at High Mach Numbers (3 to 6))." Aerodynamischen Versuchsanstalt, Gottingen, West Germany, Report 64, A29, Vol. 3, No. 7, July 1965, pp. 237-246.

13. Cable, A. J. and Cox, R. N. "The Ludwieg Pressure-Tube Supersonic Wind Tunnel." Aeronautical Quarterly, Vol. 14, No. 2, May 1963, pp. 143-157.

14. Piltz, Eckart. "Boundary-Layer Effects on Pressure Variations in Ludwieg Tubes." AIAA Journal, Vol. 10, No. 8, August 1972, pp. 1095-1097.

15. Schubauer, Galen Brandt and Tchen, C. M. Turbulent Flow, Princeton Aeronautical Paperback No. 9, Princeton University Press, Princeton, New Jersey, 1961.

16. Abbott, D. E. and Cebeci, T. "The General Analysis of Unsteady Boundary Layers - Laminar and Turbulent." Fluid Dynamics of Unsteady, Three-Dimensional and Separated Flows, Proceedings of a Project SQUID Workshop held at the Georgia Institute of Technology, F. J. Marshall, Editor, October 1971.

17. Back, L. H. "A Note on Laminar Shear Flow Over Impulsively Started Bodies." Journal of Applied Mechanics, Vol. 38, Series E, No. 4, December 1971, pp. 1065-1068.

18. Dwyer, Harry A. "Calculation of Unsteady Leading-Edge Boundary Layers." AIAA Journal, Vol. 6, No. 12, December 1968, pp. 2447-2448.

19. Tijdeman, H. and Bergh, H. "Analysis of Pressure Distributions Measured on a Wing with Oscillating Control Surface in Two-Dimensional High Subsonic and Transonic Flow." NLR-TR-F.253, March 1967.

20. Cahill, Jones F., Treon, Stuart L., and Hofstetter, William R. "Feasibility of Testing a Large-Chord, Swept-Panel Model to Determine Wing Shock Location at Flight Reynolds Number." Paper presented at the AGARD Meeting on Facilities and Techniques for Aerodynamic Testing at Transonic Speeds and High Reynolds Number, Gottingen, West Germany, April 26-28, 1971. (Found in AGARD-CP-83-71, pp. 17-1 - 17-11.)

21. Binion, T. W. Jr., and Lo, C. F. "Application of Wall Corrections to Transonic Wind Tunnel Data." AIAA Paper No. 72-1009 presented at the 7th Aerodynamic Testing Conference, Palo Alto, California, September 13-15, 1972.

22. Wehrend, William R., Jr. "An Experimental Evaluation of Aerodynamic Damping Moments of Cones with Different Centers of Rotation." NASA TND-1768, March 1963.

23. Usry, J. W. and Wallace, John W. "Drag of a Supercritical Body of Revolution in Free Flight at Transonic Speeds and Comparison with Wind-Tunnel Data." NASA TND-6580, December 1971.

24. Couch, Lana M. "Transonic Wall Interference Effects on Bodies of Revolution." AIAA Paper No. 72-1008 presented at the 7th Aerodynamic Testing Conference, Palo Alto, California, September 13-15, 1972.

25. Simon, Erwin. "The George C. Marshall Space Flight Center's 14 x 14-inch Trisonic Wind Tunnel Technical Handbook." NASA TMX-64624, November 1971.

26. Davis, John William and Graham, Robert F. "Flow Interference in a Variable Porosity Trisonic Wind Tunnel." AIAA Paper No. 72-1010 presented at the 7th Aerodynamic Testing Conference, Palo Alto, California, September 13-15, 1972.

27. Rittenhouse, L. E. and Kaupp, H., Jr. "An Investigation of the Influence of Several Shape Parameters on the Aerodynamics of Ballistic Re-entry Configuration." AEDC-TN-59-16 (AD306739), May 1959.

28. Covert, Eugene E. "A Summary of Experiments with Slotted Transonic Inserts in the Naval Supersonic Laboratory Wind Tunnel." Massachusetts Institute of Technology, Naval Supersonic Laboratory, Technical Report 207, April 1958.

29. Tirumalesa, D. and Satyanarayana, B. "An Experimental Study of the Effect of the Plenum Chamber Size on the Flow in a Slotted Wall Transonic Test Section." Journal of the Aeronautical Society of India, Vol. 12, No. 3, August 1960, pp. 51-62.

30. Anderson, C. F., Anderson, A., and Credle, O. P. "The Effect of Plenum Volume on the Test Section Flow Characteristics of a Perforated Wall Transonic Wind Tunnel." AEDC-TR-70-220 (AD876366), October 1970.

31. Estabrooks, Bruce B. "Wall-Interference Effects on Axismmetric Bodies in Transonic Wind Tunnels." AEDC-TR-59-12 (AD216698), June 1959.

32. Hartley, M. S. and Jacocks, J. L. "Static Pressure Distributions on Various Bodies of Revolution at Mach Numbers from 0.69 to 1.60." AEDC-TR-68-37 (AD828571), March 1968.

33. Robertson, J. E. "Model Study of the Exhaust Flow Noise of the Proposed AEDC High Reynolds Number Tunnel." AEDC-TR-71-146 (AD727053), July 1971.

34. Plotkin, K. J., Robertson, J. E., and Cockburn, J. A. "Environmental Impact of Noise from the Proposed AEDC High Reynolds Number Tunnel." AEDC-TR-72-151 (AD757552), October 1972.

UNCLASSIFIED

Security Classification

DOCUMENT CONTROL DATA - R & D

(Security classification of title, body of abstract and indexing annotation must be entered when the overall report is classified)

1 ORIGINATING ACTIVITY (Corporate author)

Arnold Engineering Development Center
Arnold Air Force Station, Tennessee 37389

2a. REPORT SECURITY CLASSIFICATION

UNCLASSIFIED

2b GROUP

N/A

3 REPORT TITLE

EXPERIMENTAL STUDIES OF A LUDWIEG TUBE HIGH REYNOLDS NUMBER TRANSONIC TUNNEL

4 DESCRIPTIVE NOTES (Type of report and inclusive dates)

Final Report -- July 1972 through February 1973

5 AUTHOR(S) (First name, middle initial, last name)

R. F. Starr and C. J. Schueler, ARO, Inc.

6 REPORT DATE	7a. TOTAL NO OF PAGES	7b. NO. OF REFS
December 1973	74	34

8a. CONTRACT OR GRANT NO	9a. ORIGINATOR'S REPORT NUMBER(S)
b. PROJECT NO.	AEDC-TR-73-168
c. Program Element 65802F	9b. OTHER REPORT NO(S) (Any other numbers that may be assigned this report)
d.	ARO-VKF-TR-73-92

10 DISTRIBUTION STATEMENT

Approved for public release; distribution unlimited.

11 SUPPLEMENTARY NOTES	12. SPONSORING MILITARY ACTIVITY
Available in DDC	Arnold Engineering Development Center, Air Force Systems Command, Arnold Air Force Station, Tenn.

13 ABSTRACT

A significant justification for a much higher Reynolds number ground test capability in the transonic regime has developed in the past few years. An extensive experimental investigation of a high Reynolds number transonic wind tunnel employing a Ludwieg tube air storage system has been undertaken at the Arnold Engineering Development Center to assess the utility of such a device. The transonic starting process and starting time of this impulse facility have been carefully evaluated, and the spatial and timewise quality of the test section flow has been analyzed. Results from studies of the aerodynamic flow response time at transonic speeds and measurement of the pressure distribution and forces on selected models are presented. Also included are the results from associated studies of the influence of plenum volume on test section flow quality and the acoustic environment of the tunnel exhaust.

DD FORM 1 NOV 65 1473

UNCLASSIFIED

Security Classification

14. KEY WORDS	LINK A		LINK B		LINK C	
	ROLE	WT	ROLE	WT	ROLE	WT
Reynolds number						
transonic wind tunnels						
Ludwieg tube						
pressure measurement						
boundary-layer flow						
boundary-layer growth						
flow measurement						
wind tunnel test						
Mach number						
plenum chambers						
acoustic environments						
environmental simulation						
pulsation						